μ-PIV Study of the Effect of Surfactant Concentration On the Internal Flow Fields Inside a Moving Droplet

by

Sahil Kashyap

A thesis
presented to the University of Waterloo
in fulfillment of the
thesis requirement for the degree of
Master of Applied Science
in
Mechanical Engineering

Waterloo, Ontario, Canada, 2015

Author's Declaration

I hereby declare that I am the sole author of this thesis. This is a true copy of the thesis, including the required final revisions, as accepted by my examiners.

I understand that my thesis may be made electronically available to the public.

Abstract

Droplet microfluidics has enormous potential in scientific research as well as in industrial and medical applications. Droplet microfluidics enables the generation of segments in the form of discrete fluid packets. These liquid segments are mono dispersed in a continuous phase and have wide range of applications in engineering, chemistry, biological, and medical diagnostics. Another advantage for the use of micro droplets is the fast mixing of reagents dosed inside droplets. Fast and efficient mixing of reagents in droplets strongly depends on the internal flow fields inside the droplet. Surfactants are often added to the dispersed phase to stabilize the generated droplets and prevent droplet coalescence.

This study examines the effect of surfactant concentration on the internal flow fields inside a moving droplet. Two different surfactants, SDS and Tween 20 are chosen as they allow a wide timescale of adsorption to be studied due to relative difference in their size. Micro particle imaging velocimetry (µPIV) is used in the examination of the internal flow inside the droplet. Experiments with surfactant are done in two surfactant concentrations: above CMC (critical micelle concentration) and below CMC. The study with SDS has been performed at two different droplet regimes, squeezing and transition. The effect of droplet shape is also studied by comparing the surfactant effect between slug and disk-shaped droplet. The primary difference between these shapes is the extent of liquid/wall friction between the droplet and the channel wall. It is observed that addition of surfactant to the slug droplet at low concentrations causes retardation in the internal flow, which is primarily attributed to the action of opposing Marangoni forces. Achievement of complete remobilization in the internal flow depends on surfactant type and the droplet operating regime.

Acknowledgements

First and foremost, I would like to thank my supervisor, Dr. Carolyn Ren, whose guidance and encouragement enabled me to complete my graduate studies. Her enthusiasm and passion for research is truly appreciated and her faith in me throughout has been extremely helpful and deeply acknowledged.

I am also grateful to my co-supervisor, Dr. Sanjeev Bedi, whose contribution and support during my graduate studies has been invaluable. His constant motivation and belief in me during periods of struggle encouraged me to work to the best of my abilities.

Special thanks to my thesis readers, Prof. Dongqing Li and Prof. David Johnson, for providing their valuable comments.

Many thanks to Zeyad Almutairi, my mentor for this study whose expert guidance and contribution to this study is appreciated. I am also thankful to the current members of the Waterloo Microfluidics laboratory for their valuable suggestions in this study: Gurkan Yesiloz, Cody Chen, Ning Qin and David Wong.

I am deeply grateful to my parents, who have been with me at all times during the study, for their love and support. I would also like to thank all of my friends I met in Waterloo for making life more enjoyable.

Dedication

To my parents

Table of Contents

List of Figures

List of Tables

Acronyms

CCD	Charged couple device
CMC	Critical micelle concentration
CMOS	Complementary metaloxidesemiconductor
HeNe	Helium Neon laser.
IR	Infrared.
LED	Light emitting diode.
LOC	Lab-on-a-chip
µPIV	Micro-particle image velocimetry
NA	Numerical aperture
Nd:YAG	Neodymium-doped Yttrium Aluminum Garnet laser.
PCR	Polymerase chain reaction
PDMS	Polydimethylsiloxane
PIV	Particle image velocimetry
PMT	Photomultiplier tube
SDS	Sodium Dodecyl Sulfate

Symbols

Ca	Capillary number
Re	Reynolds number
z	Plane depth (m)
h	Channel height (m)
R	Gas constant (J/mol.K)
Q_c	Flow rate of the continuous phase (m^3/sec)
kHz	Kilo-hertz
ρ	Density of the fluid (kg/m^3)
t	Characteristic time scale (sec)
U	Velocity of the fluid in the x-direction (m/sec)
V	Velocity of the fluid in the y-direction (m/sec)
L	Characteristic length scale (m)
D	Diffusion coefficient of the surfactant (m^2/sec)
μ	Viscosity of the fluid (Ns/m^2)
γ	Interfacial tension between fluids (N/m)
g	Acceleration due to gravity (m^2/sec)
Θ	Contact angle between the liquid and the solid surface
ε	Threshold for the contribution of the defocused particle on the image
δ_{corr}	Depth of correlation (m)
n_0	Index of refraction
d_p	Particle diameter (m)

M	Magnification of the objective
λ_0	Wavelength of the light (m)
Γ	Interface concentration of the surfactant (mol/L)
n	Number of solute species that change due to surfactant
T	Temperature (K)
C_1	Bulk concentration of the surfactant (mol/L)
$\hat{U}$	Internal circulation velocity (m/sec)
U_c	Circulation velocity inside the droplet (m/sec)
U_d	Velocity of the droplet relative to the fixed channel (m/sec)
a	Drop radius (m)
W_c	Width of the main channel (m)
W_{ec}	Extended width of the channel (m)
ω	Vorticity (1/sec)
F_d	Drag force (N)
τ	Time constant (sec)
K	Boltzmann constant (J/K)
D_b	Particles diffusivity due to Brownian motion (m^2/sec)

Chapter 1: Introduction

1.1 Background

Over the past decade, the area of Microfluidics has received great attention due to its enormous potential in the medical and technological applications. Microfluidics is a term coined for fluid flow in geometries which have been scaled to the micro-scale [1,2]. The scaling down of the geometry marks a shift in the governing forces for the fluid flow, from gravitational and inertial forces on the macro-scale to surface and viscous forces on the micro-scale [3]. Microfluidics offers numerous advantages over macro-scale flow in terms of reduced reagent consumption, shorter analysis time and achievement of high throughput rate [4,5]. These advantages led to the development of Lab-on-a-chip (LOC) devices and fundamental studies of physics underlying microfluidic phenomena. Over the years, LOC devices have been applied into several diversified areas, including bio-medical research, drug discovery and detection of bio weapons [6,7,8].

Generally, the material to be employed to fabricate the microfluidic device depends on the desired application. The choice of materials varies from silicon and glass to polymeric materials. Out of the materials available for fabrication, Polydimethylsiloxane (PDMS) has been extensively used for the fabrication of microfluidic chips. This can be attributed to the low cost of PDMS along with less time requirement for chip fabrication [9,10].

The application of PDMS for fabrication purposes offers several advantages, like good optical properties because of its transparency allowing for easy optical detection. Also, the surface of

PDMS can be functionally modified by the use of some chemicals and procedures to make it suitable for different applications [11]. However, there are several limitations associated with use of PDMS as well. Firstly, PDMS swells when it comes in contact with certain solvents [12]. Secondly, PDMS is soft which results in high compliance for microfluidic chips fabricated from PDMS [13]. Thirdly, Plasma treatment of PDMS for bonding with glass substrate changes the nature of PDMS from hydrophobic to hydrophilic [14,15]. This is undesirable for generating aqueous based droplets in oil phase as the surface of the channel should have preferential wetting property for the oil phase instead of the aqueous phase. However, prolonged heat treatment enables PDMS to return to its hydrophobic state [16].

A key sub-area of microfluidics is droplet microfluidics [17]. In this, droplets are generated from immiscible fluids which flow along the micro-channel. Each droplet is considered as a micro-reactor as there is no cross-contamination of reagents dosed to the droplets towards the surrounding fluid. These droplets provide high throughput as they can be generated at the kHz range along with providing accurate control over droplet volume [17,18]. As compared to single phase flow, mixing is also improved in droplets due to the formation of two counter rotating vortices inside the moving droplet [19,20]. Figure 1.1 shows an application of droplets for short tandem repeat (STR) typing for human forensic identification [21].

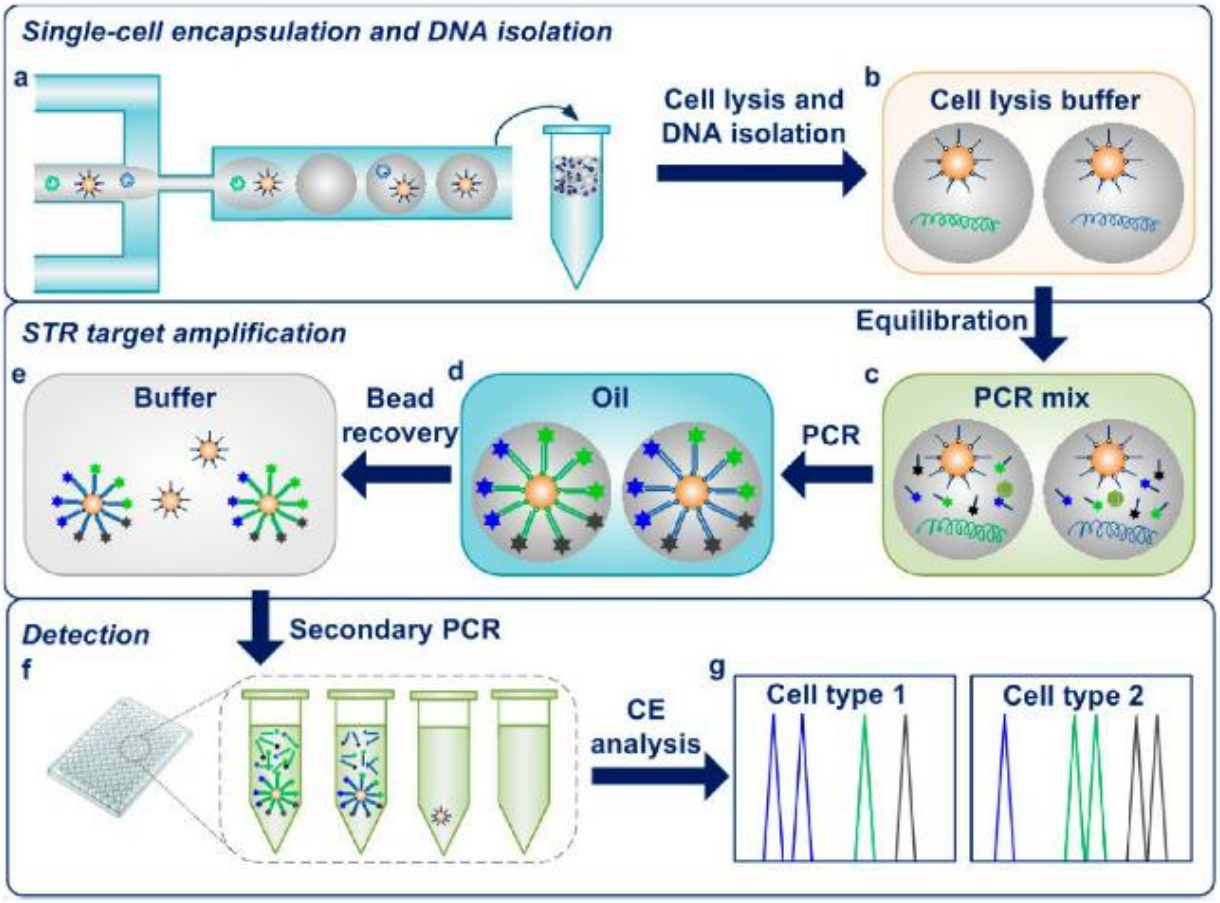

Figure 1.1: Analytical process for single-cell STR typing (a) Individual cells along with the beads are encapsulated within micro droplets. (b) Incubation of droplets for DNA isolation. (c) Equilibration in PCR mix. (d) Emulsion PCR (e) Bead recovery (f) Conducting secondary PCR (g) Use of CE system for fragment size analysis. Adapted with permission from [21]. Copyright 2014 American Chemical Society.

1.2 Research Motivation

Any chemical reaction occurring inside the droplet is affected by the mixing efficiency of the reagents dosed to the droplet. This mixing is, in turn, dependent on the internal flow fields present inside the moving droplet. Since the flow in micro-scaled geometries is laminar (Re<1), the mixing inside the droplets is likely to be diffusion controlled. But the presence of additional vortices or circulation inside the droplets would increase this mixing process significantly and hence improve the rate of chemical reaction taking place inside the droplet as well. Thus, the knowledge of the internal flow fields in the droplets enables us to have greater control over the physical phenomena occurring inside these droplets [22]. In most of the microfluidic droplet studies involving the use of surfactant, the surfactant concentration is usually taken to be way beyond the CMC value. This is done to ensure the stability of the droplets against merging which in turn, ensures complete isolation for the chemical reactions taking place inside these droplets. However, in certain applications, there might be some surfactant present in low concentrations (below CMC), in the absence of any external surfactant addition. This may be due to some impurity in the liquids used or the surfactant might have produced as a by-product in the reaction. The presence of this surfactant in low concentration would have a retarding effect on the droplet interface, thereby affecting the internal flow. This is important because the internal flow in turn affects the mixing of the reagents in the chemical reaction and determines its effectiveness.

1.3 Objectives

The goal of this study is to have a better understanding of the effect of surfactant on the flow fields inside a moving droplet. For this, μPIV technique is employed. This study aims to achieve the following objectives:

- Study the effect of increasing surfactant concentration inside the droplet on its internal flow
- Study the effect of surfactant concentration on the internal flow at a different droplet regime
- Study the effect of increasing surfactant size on the internal flow inside a moving droplet
- Comparing the effect of surfactant concentration on the internal flow by changing the droplet shape

1.4 Thesis Outline

The thesis is outlined as follows:

Chapter 2: In this chapter, literature review of droplet microfluidics along with generation of droplets is presented briefly. This is followed by detailed background literature review of internal circulation flow fields and μ-PIV approach. Finally, literature review on surfactants and their effect on the flow fields inside the droplet is presented.

Chapter 3: In this chapter, the micro-channel design used for the study is discussed. This is followed by the procedure used for fabricating the PDMS micro-channel.

Chapter 4: This chapter describes the chemicals and materials used for conducting the experiments. Also, the method for determining the interfacial tension is discussed briefly.

Chapter 5: In this chapter, the experimental system is described in detail. This is followed by discussing the experimental methodology and the PIV analysis scheme.

Chapter 6: This chapter focusses on the effect of surfactant concentration on the internal flow fields inside a moving droplet. The experimental results for different surfactants at squeezing and transition regime are discussed. Finally, the effect of surfactant concentration on droplet shape is also discussed.

Chapter 7: A summary of the major findings from the work presented in this thesis is done. An outlook of the future work is also discussed.

Chapter 2: Literature Review

2.1 Droplet Microfluidics

Two-phase flow is a very broad area investigated in the discipline of fluid mechanics. A key sub area in this field is two-phase flow in channels whose geometry is scaled to the micro-scale because microchannels allow uniform droplets or bubbles to be generated benefiting from the confinement they offer. Two phase flow in microchannel can be broadly divided into two main categories: liquid/liquid flow, commonly known as droplet microfluidics and liquid/gas flow, commonly known as bubble microfluidics. The down-scaling of the traditional two phase flow to the micro-scale adds complexity to the forces acting on the fluids in motion in the microchannel and hence affects the flow. The primary forces which govern the behavior of two phase flow in microchannel are inertia, viscous and interfacial tension. The relevance of these forces in two phase flow can be characterized by some non-dimensional numbers, which are presented in Table 2.1 [3,23].

Two phase flow in microchannel is marked by high surface to volume ratio and low flow velocities. As a consequence, the inertial and gravitational forces lose their relative importance

among the forces affecting two phase flow in microchannel. So, Bond and Weber number are usually not considered for such flows. A non-dimensional number which assumes primary importance is the Capillary number (Ca), since it describes the relationship between the viscous and the interfacial forces [23].

Table 2.1: Dimensionless numbers relevant in micro-scale two phase flow

Dimensionless #	Definition	Equation
Reynolds	Inertia/Viscous	$\frac{\rho U L}{\mu}$
Peclet	Advection /Diffusive transport	$\frac{UL}{D}$
Capillary	Viscous/Interfacial	$\frac{U\mu}{\gamma}$
Bond	Gravitational/Interfacial	$\frac{\rho g L^2}{\gamma}$
Weber	Inertia/Interfacial	$\frac{\rho U^2 L}{\gamma}$

Droplet microfluidics has been recognized to be of potential importance and significance due to its various advantages over single phase flow in microchannel. Some of the advantages include its capability for large scale combinatorial studies, size control to high accuracy, high throughput rate, extremely low volume of generated droplets (pico to nano litre) and isolation of droplets from the channel walls resulting in nearly no contamination of the reagents dosed to the droplets [17,25]. Due to the numerous advantages droplet microfluidics offers over single phase microfluidics, it has been successfully applied in several diversified areas. Prominent areas

include droplet use in measuring interfacial property [27] and fluid property [28]; application in biological studies [29,30]; improvement in mixing of viscous reagents [31] and biomedical research [32].

2.2 Droplet Generation

The generation of droplets in microchannel can be achieved through various channel designs. Some of the prominent designs include T-junction, flow focuser and parallel flow (Figure 2.1). The phase which carries the droplet is referred to as the “continuous phase”, while the droplet itself is referred to as the “dispersed phase”. The generation of droplets is determined by the imbalance in the forces maintaining the dispersed phase flow. This leads to the rupturing of the interface of the dispersed phase by the continuous phase, leading to the formation of the droplets. After the formation, the droplets move along the microchannel along with the continuous phase [24].

2.2.1 T-junction generator

There are certain key criteria defined for stable generation of droplets in a microchannel [34,35]. The microchannel design with higher hydrodynamic resistance downstream showed improved droplet stability. Another criterion that resulted in the stable generation of droplets in a T-junction generator is that the resistance of the channel supplying the dispersed phase is increased to be nearly the same order as that of the downstream channel [34].

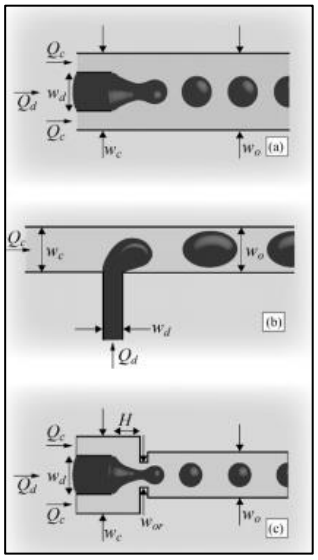

Figure 2.1: Three different geometries used for generation of droplets (a) Co-flowing streams (b) T-junction generator (c) flow focusing geometry. Adapted from [33] with permission.

T-junction generator is extensively used for the generation of microfluidic droplets [25,36]. In a T-junction generator, the continuous fluid flows in the main channel and the dispersed phase enters this channel from a branching channel. The entrance of the dispersed phase blocks the main channel fully or partially, and results in the imbalance of fluid forces between the two phases. This imbalance leads to the rupturing of the interface of the dispersed phase, resulting in the formation of droplets. A schematic illustration of a T-junction generator in a rectangular micro-channel is shown in Figure 2.2.

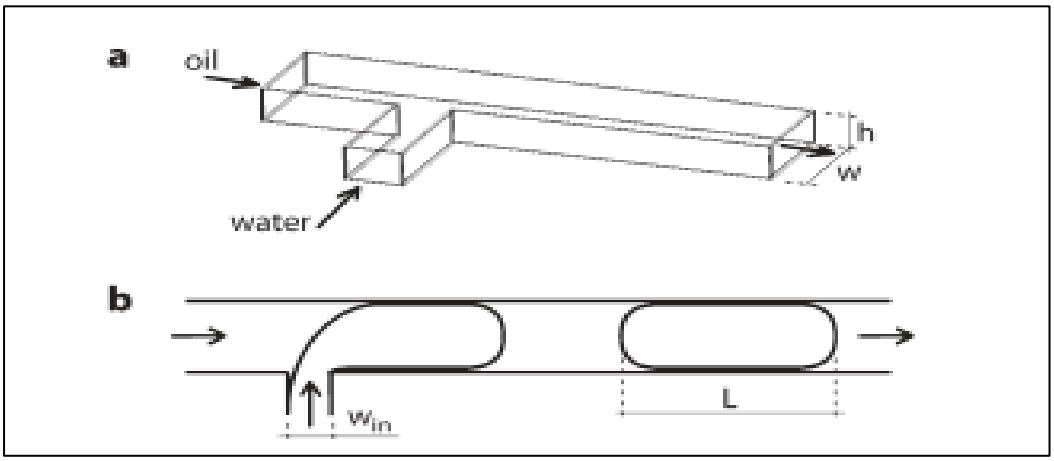

Figure 2.2: (a) Schematic illustration of T-junction in a rectangular microchannel having width w and height h. (b) Top view of the schematic shown in (a). Dispersed phase is introduced from branching channel having width w_{in}. Adapted from [37] with permission of The Royal Society of Chemistry. http://dx.doi.org/10.1039/B510841A

The operating regimes of droplet generation in a T-junction generator can mainly be divided into three categories: squeezing, transition and dripping [38,39]. These three regimes differ in the force that is responsible for the generation of droplets. The force responsible for droplet generation for each regime along with the range of Ca is shown in Table 2.2.

Table 2.2: Operating regime of droplet generation in a T-junction generator [38]

Regime	Force	Ca
Squeezing	Pressure	Ca < 0.002
Transition	Pressure and Shear	0.002 < Ca < 0.01
Dripping	Shear	0.01 < Ca <0.3

2.2.2 Fluid pumping system

There are mainly two types of fluid pumping systems used in microfluidics – pressure system and syringe pumps. The pressure system operates by applying a constant pressure difference across the inlet and outlet sources in a microchannel, resulting in a flow in the microchannel. The pressure system is reported to have greater stability in generating uniformly sized droplets with equal spacing between the droplets, as compared to the syringe pumps by Korczyk et al [40]. This is attributed to the fact that flow in the microchannel achieves a steady condition by adapting to the constant pressure difference applied across the microchannel. In addition, the pressure system has no moving parts, which also contributes to the stability of the droplets in the microchannel.

On the other hand, the syringe pumps operate by movement of the lead screw through the use of electric motors. This motion of the lead screw drives the syringes, which results in pumping of fluid into the microchannel. It is worth mentioning that although the pressure system results in more stable droplet generation as compared to the syringe pumps, proper choice of the syringe diameter corresponding to the desired flow rate results in stable generation of droplets from the syringe pumps as well.

2.2.3 Wetting of Surfaces

Wetting of a surface by a fluid is generally defined as the displacement from a surface of a fluid by a different fluid. Thus, wetting always involves three phases, of which at least two are fluids [41]. When the liquid is brought into contact with the solid surface, there are some possible outcomes. The first is that the liquid will completely spread on the surface, resulting in a contact angle of 0^0. This condition is referred to as perfect wetting. The other outcome is that the liquid doesn't completely spread on the surface, but instead forms an angle with the surface. This condition is referred to as partial wetting [42]. Partial wetting can further be divided into two conditions – high and low wettability. When the surface favors the liquid and the contact angle between the liquid interface and the surface is less than 90^0, the condition is referred to as high wettability. On the other hand, when the contact angle is greater than 90^0, the condition is referred to as low wettability.

Wetting of surface is an important property that determines the stable generation of droplets in a microchannel. For water, a highly wetted surface is also termed as hydrophilic and otherwise hydrophobic. The condition that is crucial for generating uniform droplets by the continuous phase is that the surface of the microchannel should be hydrophobic, with the contact angle between the channel and the liquid interface to be at least 135^0 [36,43]. PDMS is the most common material used for the fabrication of microchannel. Silicone oil is the preferred choice to be used as the continuous phase with PDMS microchannel, because of its natural property of preferentially wetting of PDMS. But during the fabrication of PDMS microchannel, it is plasma treated to be bonded with another substrate [9,14]. One implication of this plasma bonding is that

it converts the PDMS surface from hydrophobic state to hydrophilic state, which is not desired for stable generation of droplets in the microchannel. The reversion of the PDMS surface to hydrophobic state is achieved by heating the PDMS surface for a long period of time [44]. Consequently, achieving the proper wetting conditions for PDMS leads to stable droplet generation in the microchannel. This can be confirmed by observing the shape of the leading and trailing caps of the droplet. Proper wetting conditions lead to nearly hemi-spherical surface at the droplet's leading and trailing edge. On the contrary, poor wetting conditions would result in droplets sticking to the channel walls, leading to unstable droplet generation.

2.3 Internal circulation flow fields

2.3.1 Introduction

The knowledge of internal flow inside droplets is of great importance in the field of droplet microfluidics. The internal flow in droplets significantly affects mixing of reagents which in turn affects the chemical reaction taking place inside the droplet. Since the flow in micro scaled geometries is laminar, the mixing inside the droplets is likely to be diffusion controlled. But the presence of additional vortices or circulation inside the droplets would increase this mixing process significantly and hence improve the rate of chemical reaction taking place inside the droplet as well. Thus, the knowledge of the internal flow fields in the droplets enables us to have

greater control over the physical phenomena occurring inside these droplets [22]. µPIV, due to its high spatial resolution, has emerged as a powerful tool for observation of internal flow fields.

2.3.2 µPIV approach

µPIV approach is a very suitable technique which can be employed for visualization of the internal flow inside the droplets moving in a microchannel. Basically, µPIV is a term given to the application of the well-known Particle Image Velocimetry (PIV) technique to the geometries scaled down to the micro scale [1,45]. PIV has been long established as a credible experimental technique for visualization of flow in enclosed and open systems [46,47].

The working principle of PIV is briefly described here. The fluid is uniformly loaded with tracer particles, which are assumed to follow the flow completely. The displacement of these particles is determined by shining these particles by a suitable light source and acquiring two consecutive images with a known time difference between them. The time difference is kept small so that any errors arising from the acceleration of the particles are minimum. Applying the cross-correlation on these two consecutive images gives the desired two dimensional Lagrangian velocity field. For a small interrogation area, this is mathematically represented as [45]:

$$u_{(i,j)} = \frac{\Delta x_{(i,j)}}{\Delta t} \tag{2.1}$$

where (i,j) represents the position of the interrogation area in the flow field, $u_{(i,j)}$ is the component of velocity in the x-direction , $\Delta x_{(i,j)}$ is the displacement of the tracer particles in the x-direction and Δt is the time difference between the recorded images. On similar lines, the y-

component of the velocity, $v_{i,j}$, can be determined, which leads to obtaining the two-dimensional velocity vector $V_{(i,j)}$ at the position (x_i, y_j) as [45]

$$V_{(i,j)} = u_{(i,j)} + v_{(i,j)} \tag{2.2}$$

There are some underlying obstacles on the application of PIV to the micro-scale geometries. One prominent obstacle is that a sheet of laser which generally illuminates only a plane in PIV on macro-scale, illuminates the entire volume in micro scale geometries. Additionally, the typical tracer particles used in PIV do not scatter sufficient light in micro scale geometries in order to observe their displacement. These two obstacles are removed by the use of fluorescence microscopy [45,48]. The passage of light through microscope objective lens enables recording of light sheet by the camera. The use of fluorescent particles emits sufficient light to be detected by the image sensor (Figure 2.3).

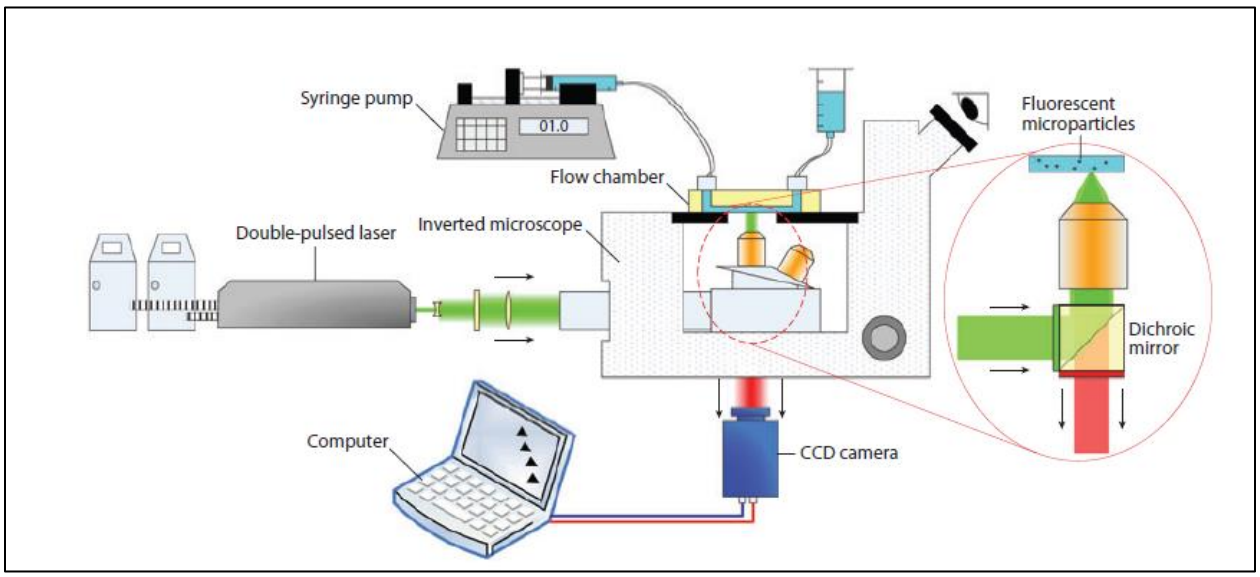

Figure 2.3: Schematic of a μPIV apparatus using fluorescent microscopy. Fluorescent particles are excited by the illuminating light from double pulsed laser, which emit light which passes through a mirror and then recorded by a CCD camera. Adapted from [49] with permission.

μPIV has been recognized as a great tool to characterize flow inside droplets moving in a microchannel. However there are some challenges in applying μPIV for observing internal flow inside droplets. Firstly, there exists a difference in the refractive index between the continuous and the dispersed phase. This mismatch results in distortion of light path when it crosses the liquid interfaces, leading to regions having large light distortions within the recoded images, which affect the accuracy in the results for velocity fields obtained from μPIV [50]. Kim et al.[51] examined another effect of refractive index mismatch. They reported that there is a difference between the actual and desired focus plane, when the light passes through two liquids with different refractive indices.

Hence, it is important to match the refractive indices of different liquids, prior to the use of μPIV. This can be achieved by the suitable addition of some liquids to the liquid whose refractive index needs to be matched. Some of the liquids used for changing the refractive index of water based solutions are glycerol, sodium iodide and zinc iodide [52].

Another challenge in the application of μPIV for droplet studies is the averaging of the results [24,48]. The advantage of averaging the results in μPIV is that it reduces the errors related to the measurements of velocity fields. The challenge of averaging the results arises from the fact that it is impractical to record multiple images of the same droplet and then average the results. This challenge is overcome by taking benefit of one of the advantages of droplet microfluidics of generation of mono-disperse and uniform droplets. So, multiple droplets which are generated at the same steady condition and the same phase are averaged, instead of recording the images of the same droplet at multiple positions. This method is attributed as the phase-locking of droplets [53,54].

In typical microscopy, in principle, the particles that are present only in the depth of field of the objective lens are focused at and are recorded by the camera. But in µPIV, the out of focus fluorescent particles may also be recorded and potentially affect the velocity field measurements. This condition is known as the depth of correlation. Mathematical expression for determining the depth of correlation is given as [55]

$$\delta_{corr} = 2\left[\frac{(1-\sqrt{\varepsilon})}{\sqrt{\varepsilon}}\left(\frac{n_o^2 d_p^2}{4(NA)^2} + \frac{5.95(M+1)^2\lambda_o^2 n_o^4}{16M^2(NA)^4}\right)\right]^{1/2} \tag{2.3}$$

where δ_{corr} is the depth of correlation, ε is a threshold for the contribution of the defocused particle on the image, n_o is the immersion medium index of refraction , d_p is the particle diameter, NA is the numerical aperture of the objective lens, M is the magnification of the objective, λ_0 is the wavelength of the light.

The above discussion is an attempt to present the basic principle of PIV and key points related to the application of µPIV technique. For further insight into the principle of PIV and µPIV, Raffel et al [45] and Nguyen and Wereley [1] are recommended. Different approaches on employing the PIV and µPIV technique for different applications and developments can be reviewed through Lindken et al [48] and Wereley and Meinhart [49].

Shinohara et al [56] reported the first application of high speed µPIV to examine a two immiscible liquid/liquid flow. They examined the cross stream flow condition to study the dynamic behavior of the two immiscible liquids, Butyl Acetate and Water. They used a continuous wave laser as the light source and a high speed CMOS camera as the image sensor.

The diameter of the fluorescent particles added was 1 μm and they were added to the water phase only. They observed the creation of vortices at the liquid/liquid interface and associated this formation of vortices to the instability at the interface between the two immiscible liquids.

After the successful application of μPIV to examine the two phase flow, it has since been applied to several studies in droplet microfluidics to obtain the flow fields at the T-junction generator[53], as well as inside the droplets moving in straight and curved channels [57,58].

2.3.3 Internal Flow fields

The knowledge of internal flow inside droplets is important in the field of droplet microfluidics. The internal flow in droplets affects mixing of reagents which in turn affects the chemical reaction taking place inside the droplet. Since the flow in micro scaled geometries is laminar, the mixing inside the droplets is likely to be diffusion controlled. But the presence of additional vortices or circulation inside the droplets would increase this mixing process significantly and hence improve the rate of chemical reaction taking place inside the droplet as well. Thus, the knowledge of the internal flow fields in the droplets enables us to have greater control over the physical phenomena occurring inside these droplets [22]. Kinoshita et al [22] examined the three-dimensional internal flow fields inside droplets using confocal μPIV. The advantage of confocal microscopy over regular μPIV is negligible effect of out of focus particles on the recorded images and improved vertical measurement resolution, which helps in three dimensional velocity measurement. They generated droplets in a T-shaped microchannel using Silicon oil as the continuous phase and Water-glycerol mixture solution as the dispersed phase. They added fluorescent particles (d_p=500nm) to the dispersed phase only in order to examine its

velocity fields. A continuous wave diode laser was used as the light source and a high speed CMOS camera for recording the images. The schematic diagram of expected three dimensional flow around the droplet surface from the measurement results is shown in Figure 2.4.

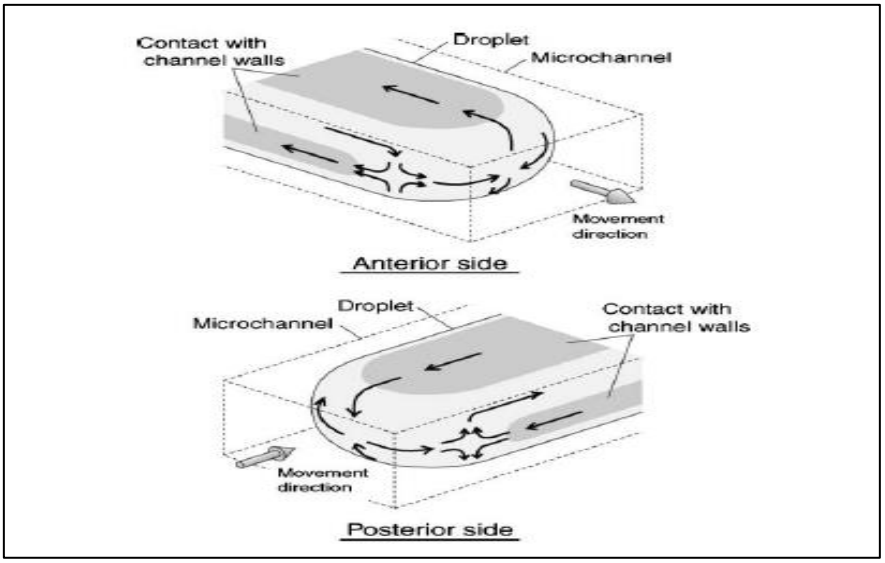

Figure 2.4: Schematic diagram of expected flow around the droplet surface from the measurement results. Adapted from [22] with permission of The Royal Society of Chemistry. http://dx.doi.org/10.1039/B617391H

The droplet surface in contact with the channel walls is dragged backwards, whereas the droplet surface near the corner regions of the channel (also referred to as the gutter region) is moving forward. This is attributed to free slip between the two phases at the liquid/liquid interface in the gutter region. Since the dispersed phase fluid is trapped within the enclosed volume of the droplet, it is forced to spread within the droplet resulting in a circulating flow within the droplet [22].

Figure 2.5 shows the cross sectional flow fields at the depth-wise middle plane of the droplet i.e. z/h = 0.5. It can be observed that near the channel wall, the flow inside is backwards, which is due to the drag between the walls and the droplet surface. However, the flow in the core of the droplet is moving forward along the direction of movement of the droplet. This creates a circulation flow at this cross section of the droplet, which results in the formation of two vortices inside the droplet [22].

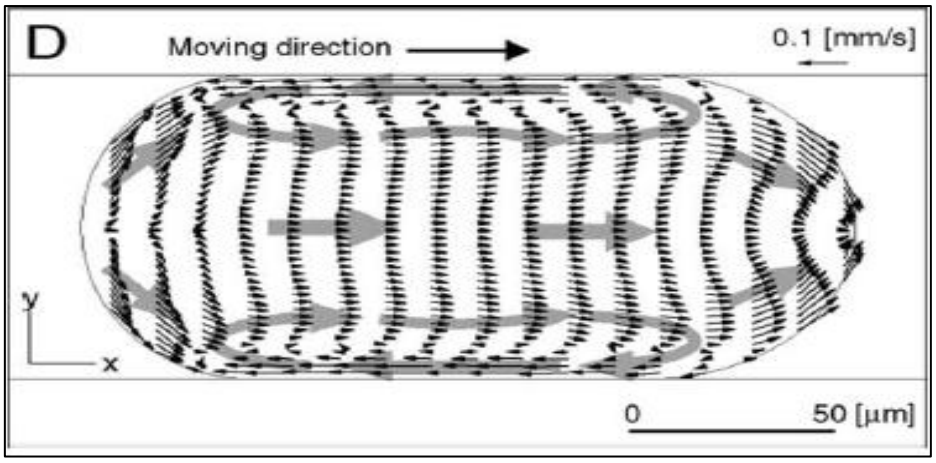

Figure 2.5: 2D velocity distributions at the center cross-section of the droplet. Adapted from [22] with permission of The Royal Society of Chemistry. http://dx.doi.org/10.1039/B617391H

Another µPIV study on the internal flow of droplets moving in winding microchannels is performed by Malsch et al [58]. They utilized all glass microchannel using tetradecane as the continuous phase and water as the dispersed phase. Yeast cells having diameter of 4-5 µm were used as the tracer particles. Red high-power LED was used as the light source and a high speed CMOS camera was used to record the images. They reported that the internal flow fields inside droplets are mainly induced due to friction at the interfaces, which has two contributing factors: liquid/wall friction and liquid/liquid friction. The internal flow fields for water/oil segments are

determined by the liquid/liquid friction, whereas for water/air system, these are determined by the liquid/wall friction. This is attributed to the fact that lower magnitude of viscosity of air results in lower interface friction between water/air system as compared to water/oil system. Another observation is that the movement of droplets through winding channel leads to the formation of asymmetric flow patterns inside the droplet as compared to the linear channel. This in turn results in complex flow fields with improved mass transfer and mixing efficiency over the droplet.

2.4 Surfactants

2.4.1 Introduction and Importance

Surfactants are amphiphilic molecules, meaning that they contain both hydrophilic and hydrophobic parts at their respective terminating ends. In two phase flow, where two immiscible fluids are in contact with each other, surfactants adsorb at the interface between the two fluids where the hydrophilic part gets oriented towards the aqueous phase and the hydrophobic part towards the oil phase. This particular orientation of the surfactant on the interface results in reduction of the surface tension between the two fluids [59].

There are certain parameters of surfactant which are significant in the area of droplet microfluidics, like Critical micelle concentration (CMC), interface coverage by the surfactant, and the diffusion time. CMC is defined as the concentration of the surfactant at which micelles start appearing in the bulk of the surfactant. Above CMC, micelles and monomers exist in

dynamic equilibrium with each other [60]. This is generally marked by a sharp change in the slope of the graph between the interfacial tension and the concentration of the surfactant. This is shown in Figure 2.6. As can be observed, the decrease of interfacial tension with increasing surfactant concentration follows a linear trend till the concentration reaches the CMC. After that, there is very less decrease in interfacial tension with further increase of concentration beyond the CMC. The region below the CMC is marked by only the presence of surfactant monomers, whereas above CMC both micelles and monomers exist in equilibrium with each other.

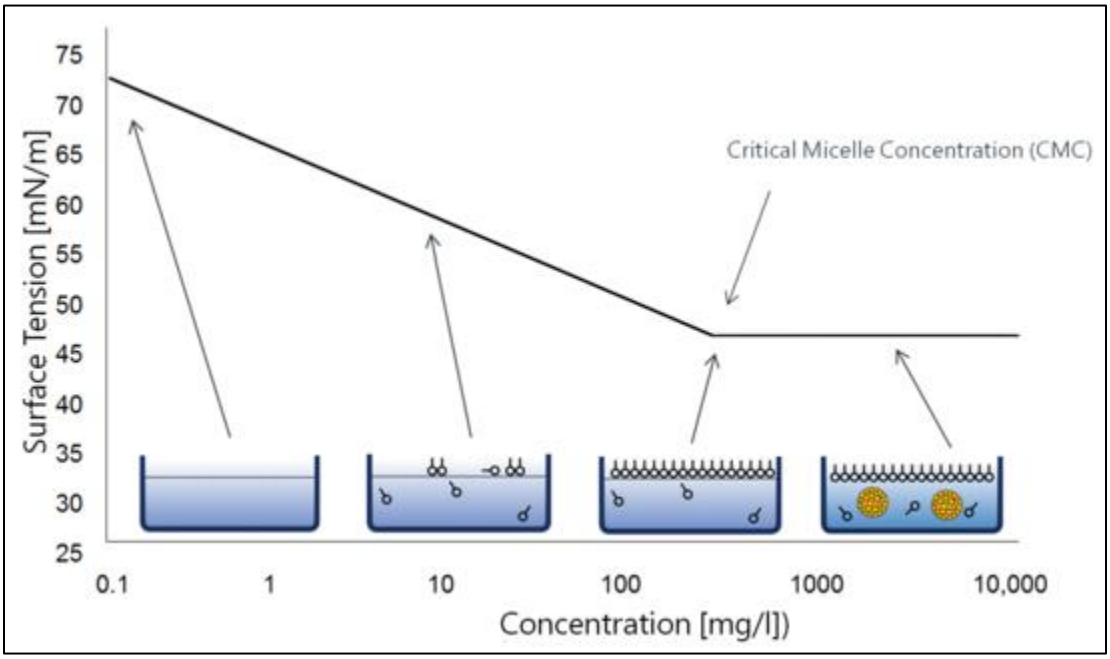

Figure 2.6: Variation of surface tension with increasing concentration of surfactant. Adapted from [61] with permission.

The decrease of the interfacial tension is directly affected by the interfacial coverage by the surfactant. The interfacial coverage is dependent upon the surface and bulk concentration of the surfactant, as well as the diffusion time scale of the surfactant. Mathematically, the interface coverage by the surfactant based on Gibbs energy equation is represented as [62]:

$$\Gamma = -\frac{1}{2.303\, nRT}\left(\frac{\partial \gamma}{\partial log C_1}\right)_T \tag{2.4}$$

where Γ is the interface concentration of the surfactant, R is the gas constant, n is the number of solute species that change due to surfactant's presence ,T is the temperature, γ is the surface tension and C_1 is the bulk concentration of the surfactant. The diffusion time is defined as the time required by the surfactant molecule to diffuse to the interface. The diffusion time is influenced by various factors like the kinetics of adsorption and desorption of the surfactant at the interface, and the micellar break up kinetics of the surfactant [62]. Mathematically, the diffusion time for simplified case of surfactant molecule diffusion is given as:

$$t = \frac{L^2}{D} \tag{2.5}$$

where t is the time required by the surfactant molecule to diffuse to the interface, L is the distance covered by the surfactant and D is the diffusion coefficient of the surfactant. Surfactants inside moving droplets are transported by the fluid flow (convection) and by diffusion, in the bulk, as well as along the interface.

Surfactants play a crucial role in the area of droplet microfluidics. Due to the adsorption of surfactant molecules at the interface of the droplet, the addition of surfactant provides stability to the droplets against coalescence (Figure 2.7). This is because the presence of surfactant molecules at the interface would not allow the droplets to come in contact with each other, thus preventing any chances of droplet mixing. This is very useful in droplet microfluidic applications, as the presence of surfactant assures the stability of the system and no droplet merging. This, in turn, allows complete isolation and non-contamination to any chemical reaction taking place inside the droplets. Thus, to a large extent, the use of surfactants is of prime

importance in assuring the stability of the chemical reactions inside the droplet. In other words, "real application" in the field of droplet microfluidics is very difficult and challenging to perform without the use of surfactants. It should be pointed that most of the applications involving surfactants are performed at surfactant concentration way beyond the CMC value. This is done to so that the interface coverage is nearly full, which assures complete stability of the droplets.

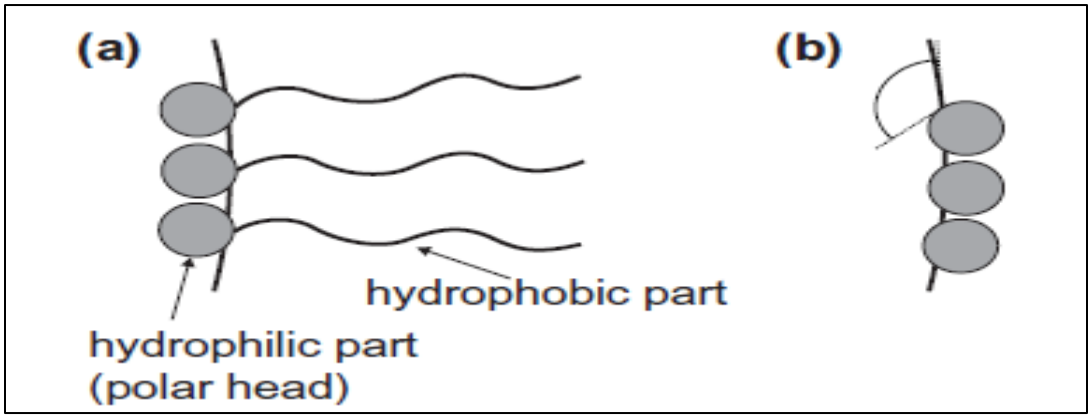

Figure 2.7: Schematic of stabilizing property of a surfactant (a) having a hydrophobic tail and a polar head (b) Contact angle gives the orientation at the fluid/fluid interface. Adapted from [63] with permission.

2.4.2 Surfactants on internal flow

Stebe et al [64,65] performed a two part study for understanding the effect of surfactant on fluid particle interface retardation. They reported that surface mobility in the presence of a surfactant is affected by two factors: (1) the action of Marangoni stresses and (2) Intrinsic surface rheology due to interface coverage by the surfactant.

In the first part of the study, Stebe et al [64] generated a three phase slug flow of fluorocarbon oil (FC 43,3M), water and air in a Teflon capillary tube. They attached two pressure taps at the

upstream and downstream of the test section to measure the pressure drop. The surfactants that were added to the water phase were Triton X-100, Brij 35 and bovine serum albumin (BSA). They reported that desorptive and bulk diffusive resistances are responsible for collection of surfactant at the fluid particle surface. In order to remove these two resistances, two conditions need to be satisfied. Firstly, the desorption rate of the surfactant has to be fast in comparison to the convection rate at which the surfactant is getting collected on the fluid interface inside the droplet. Due to the presence of micelles above CMC, one restriction gets added to this condition that the micellar-monomer exchange must also be rapid as compared to convection rate. Secondly, the bulk concentration of the surfactant has to be high enough so that the bulk diffusive resistances are removed. They used pressure drop as a parameter to study the interfacial retardation effects as a decrease in the interface mobility would result in large shear stresses at the fluid interface, resulting in increase of pressure drop to maintain constant velocity of the slug train. They observed that for both Triton X-100 and Brij-35, increasing the concentration of the surfactant initially increased the pressure drop to a maximum value. This was attributed to the significant bulk diffusive resistance present at low concentration of surfactant (below CMC), which led to the accumulation of surfactant molecules at the rear stagnation zone of the aqueous slug interface. This gives rise to Marangoni surface traction which is in a direction opposite to the flow and hence, reduces the surface velocity. After reaching a particular concentration of the surfactant, the pressure started decreasing and ultimately, attained the initial value. This was attributed to the elimination of the bulk diffusive resistances which were present at low concentration of the surfactant.

Assuming high desorption kinetics of the surfactant, the interface and the adjoining sublayer exist in equilibrium with each other. As the bulk concentration of the surfactant is increased to reach the CMC value, micelles start appearing which exist in equilibrium with the monomers. At the converging surface stagnation point, accumulated monomers which are swept here due to surface convection get incorporated into micelles due to the micelle-monomer equilibrium. Thus, at this end, there is no excess concentration of the surfactant. On the other end, the surface convection sweeps the monomers away from that region. This locally leads to the concentration reaching below CMC in that region, which results in the formation of micelle free zones. This leads to loss of monomers from this end as there are no micelles present in the sublayer to replenish the swept monomers. As a result of this, concentration gradient exists across the aqueous slug, leading to Marangoni stresses which retard the interfacial flow. As the bulk concentration is further increased beyond CMC, the micellar concentration increases, which results in shrinkage and eventual disappearance of the micelle-free zones. This would lead to uniform concentration of surfactant across the aqueous slug interface and thus attainment of complete remobilization of internal flow. Complete remobilization was possible for both Triton X-100 and Brij 35 because of their fast desorption kinetics and fast monomer-micelle kinetics [64].

However, the results for BSA showed that remobilization was not observed at all. This was primarily attributed to the multilayer formation and slow desorption kinetics of BSA protein as compared to the internal convection rate. In this case, the BSA protein adsorbs to the interface and gets convected to the converging stagnation point. Since the rate of desorption is slower as compared to the convection rate, the surfactant would keep on accumulating here, resulting in

higher surfactant concentration gradients, which lead to higher surface tension gradients and eventually, higher Marangoni stresses [64].

In the second part of the study [65], they used the same three phase slug flow geometry. They showed that a prior retardation of the interface because of a surfactant can be removed by the addition of a remobilizing surfactant in ample quantity. They used bovine serum albumin (BSA) protein and low concentration of Brij 35 as retarding surfactants and Triton X-100 as the remobilizing surfactant. To illustrate the retardation phenomena, they took the simple case of a spherical droplet falling slowly in another immiscible liquid. As the droplet attains the terminal velocity, the surrounding liquid flows around it. When the surfactant concentration is well below the CMC, the bulk diffusive resistances are high as bulk diffusive flux is proportional to the bulk concentration of the surfactant. Surfactant is swept away faster at the leading edge of the droplet than can be replenished by diffusion, leading to depletion of surfactant here. At the trailing edge, surfactant is brought faster by convection than can be diffused away, leading to accumulation of surfactant here. This leads to a gradient in concentration of surfactant, which results in surface tension gradient across the droplet. The region with high surface tension pulls the low surface tension region towards it, which retards the internal flow by exerting Marangoni stress along the interface. This is shown in Figure 2.8 [65].

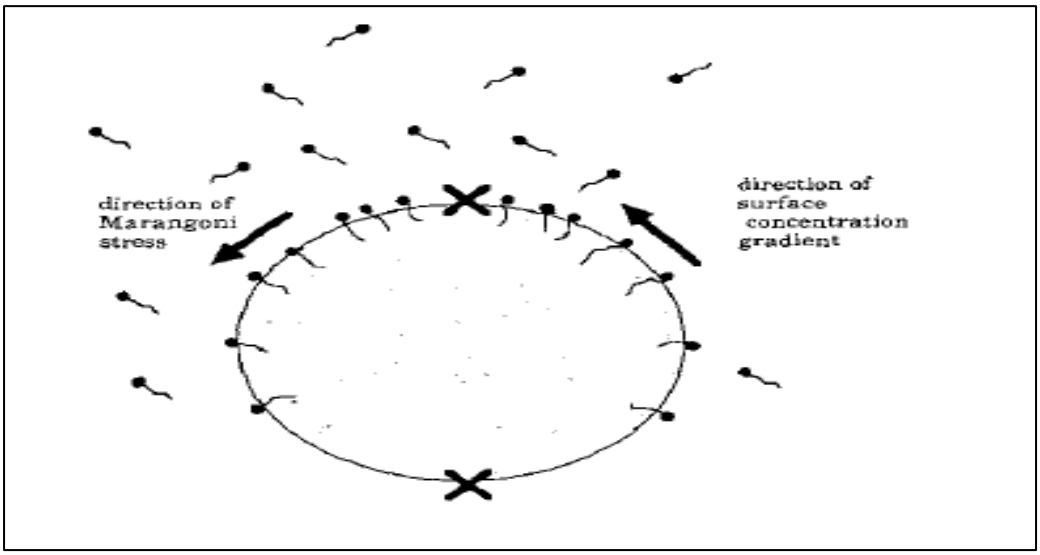

Figure 2.8: The distribution of surfactant well below the CMC, and the resulting Marangoni stress on the interface of a spherical droplet settling at its terminal velocity. X shows the stagnation points. Reprinted from [65], with permission from Elsevier.

As the concentration of surfactant is increased and approaches the CMC value, the surfactant is still present in the monomeric form. But accumulation of surfactant at the trailing edge increases the concentration of surfactant to above CMC locally at the sublayer. This results in formation of micelles at this zone, which results in excess monomers getting incorporated into micelles in this region due to the monomer-micelle equilibrium. This maintains a uniform concentration of the surfactant at this edge, provided that the rate of micelle-monomer incorporation is faster than the surface convection rate. However, at the leading edge, the surfactant is still getting swept faster than can be replenished by diffusion. Consequently, a gradient in surfactant concentration exists, which ultimately leads to Marangoni stress and interfacial flow retardation. This is shown in Figure 2.9 [65].

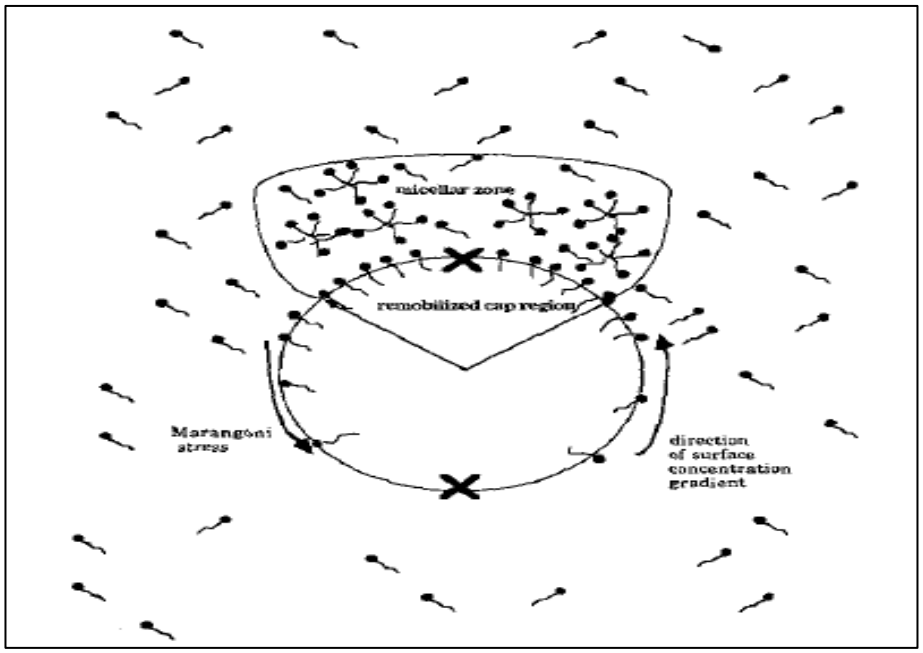

Figure 2.9: The distribution of surfactant just below the CMC, and the formation of a micellar zone at the trailing edge of the spherical droplet settling at its terminal velocity. X shows the stagnation points. Reprinted from [65], with permission from Elsevier.

Eventually, as the concentration of the surfactant is increased to slightly above CMC value, both monomers and micelles exist in equilibrium with each other. At the leading edge of the droplet, the surfactant is swept away by the surface convection. This leads to a decrease in surfactant concentration to below CMC locally in this region. This causes the micelles to dissociate and appearance of a micelle free zone in that region. So, in this region, there are no micelles present underneath to replenish the loss of monomers from this region. So, there is a depletion of surfactant at the leading edge of the droplet. However, micelles are present underneath at the trailing edge of the droplet. Excess monomers at the trailing edge of the droplet get incorporated into micelles, which maintain uniform monomer concentration at their CMC value. The

remobilized cap region increases farther away towards the leading edge in this case, but near the leading edge, surfactant concentration gradient still exists. This is shown in Figure 2.10 [65].

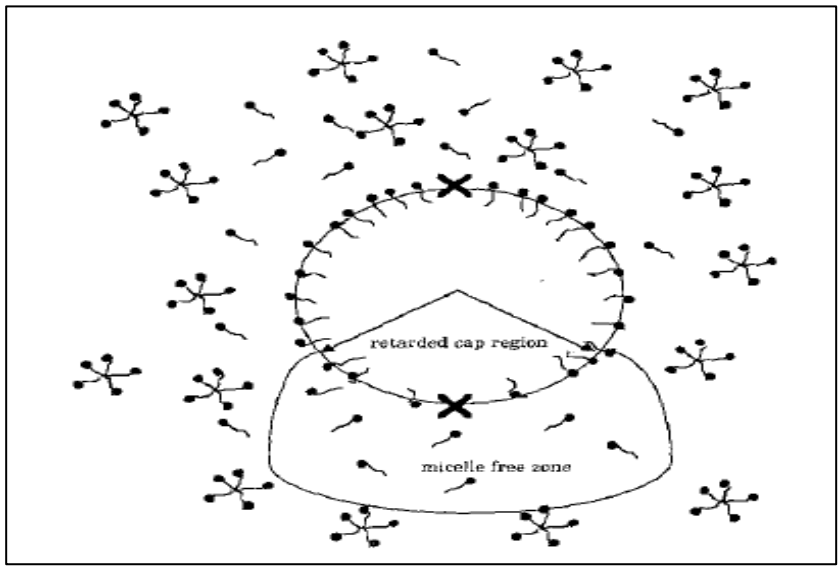

Figure 2.10: The distribution of surfactant above the CMC, and the formation of a micellar free zone at the leading edge of the spherical droplet settling at its terminal velocity. X shows the stagnation points. Reprinted from [65], with permission from Elsevier.

Ultimately, as the surfactant concentration is gradually increased to way beyond the CMC value, the micelle free zone would keep on shrinking and ultimately disappear. This would result in attainment of uniform surfactant concentration across the droplet interface. This implies that no surface tension gradient would be present and consequently, no Marangoni stress acts along the interface. This leads to complete remobilization of the droplet interface.

To study the remobilization process, they fixed the concentration of the retarding surfactant which provided maximum retardation, and then gradually increased the concentration of the remobilizing surfactant. They observed that for both cases of retarding surfactants (low concentration of Brij 35 and BSA protein), the pressure drop required to drive the slug train

remained elevated and attained a maximum value just below the CMC for Triton X-100. Further increase in the concentration of Triton X-100 to above CMC values decreased the pressure drop to ultimately attaining the pressure drop required to drive the clean slug flow, implying complete interface remobilization.

Similar observations regarding the interfacial retardation by Marangoni effects were reported by Martin and Hudson [66]. They produced water droplets in mineral oil using n-butanol as the surfactant. They used internal circulation velocity, Û in the droplet as a parameter to quantify circulation inside the spherical droplet. Mathematically, Û is represented as

$$\hat{U} = \frac{\frac{U_C}{U_d}}{(\frac{2a}{h})^2} \tag{2.6}$$

where U_c is the circulation velocity inside the droplet, U_d is the velocity of the droplet relative to the fixed channel, a is the drop radius and h is the channel height. They observed significant interfacial retardation at low surfactant concentration and a decrease in the interfacial retardation as the surfactant concentration is increased.

In most of the microfluidic droplet studies involving use of surfactant, the surfactant concentration is usually taken to be way beyond the CMC value. This is done to ensure the stability of the droplets against merging which in turn, ensures complete isolation for the chemical reactions taking place inside these droplets. However, in certain applications, even in the absence of any surfactant addition, there still might be some surfactant present in low concentration. This may be due to some impurity in the fluids or the surfactant might have produced as a by-product in the reaction. The presence of this surfactant in low concentration would have a retarding effect on the droplet interface, thereby affecting the internal flow. This is

crucial because the internal flow, in turn affects the mixing of the reagents in the chemical reaction and affects its effectiveness. This study attempts to observe the effect of surfactant concentration on the internal flow fields inside slug droplet using µPIV technique. For this, two different surfactants, SDS and Tween 20 are chosen because their use provides a wide range of diffusion time scales to be investigated [67].The study is performed at two different droplet generation regimes (squeezing and transition). Finally, the shape of the slug is changed to disk-shaped droplets and the effect of surfactant concentration on their internal flow is investigated.

Chapter 3: Microchannel design and fabrication

3.1 Microchannel design

The design used for the generation of slug droplets is shown in Figure 3.1. The width of the main channel (W_c) is 200 µm and the height is 150 µm. The droplets are generated at the T-junction and are detected downstream at the straight section of the channel. Increased resistance path is provided to the dispersed phase to ensure the stability of the droplets. Waveguides are provided in the design for insertion of fiber optics to detect the droplets. In the later part of our study, this design is modified to generate disk-shaped droplets. The aim of this design modification is to generate droplets which have circular cross-section just touching the channel walls and moving with the same velocity as the slug droplet. For this, the main channel width is extended just after the slug droplet is generated completely at the T-junction (Figure 3.2). This ensures that the disk-shaped and slug droplet would have the same volume and there would be no prior effect of surfactant accumulation inside the disk-shaped droplets. The width of the extended channel (W_{ec}) is calculated by equating the volume of the slug droplet with the disk-shaped droplet and determining the diameter of the disk-shaped droplet. The extended width was estimated to be between 280-300 µm. So, designs with extended width ranging from 275-330 µm with increments of 3 µm in width were prepared to incorporate the variations in estimating droplet

curvatures and PDMS channel swelling by the silicone oil. After numerous trials, the extended width of the channel (W_{ec}) for which the circular cross section of the droplet is just in contact with the channel walls is found to be 297 µm.

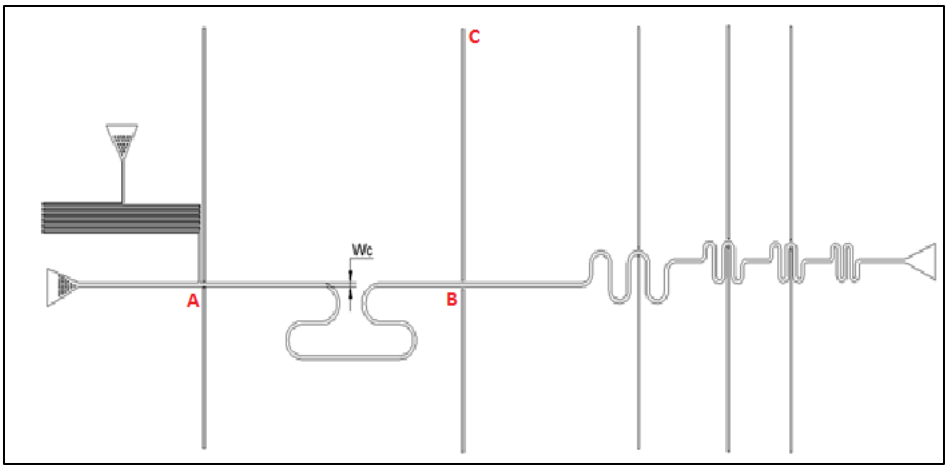

Figure 3.1: Micro-channel design for slug droplet. Droplets are generated at A and detected at B. Waveguides are provided at C for fiber insertion

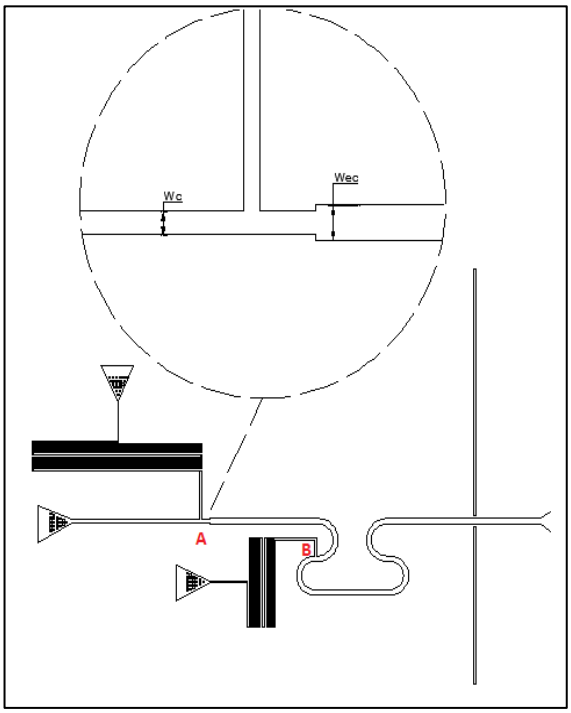

Figure 3.2: Micro-channel design for disk-shaped droplet. Droplets are converted from slug to disk shaped at A. Diluting stream is added at B to maintain same droplet velocity as the slug case.

It can be observed that the effect of dilation is negligible as disk-shaped droplets are formed just after slug formation. There is no prior interface coverage of surfactants as the interface has just formed. Also, a diluting stream is added which would ensure that the disk –shaped droplets travel with the same velocity as the slug droplet at the time of acquisition.

3.2 PDMS micro-channel fabrication

Soft-lithography technique is used for fabricating silicon master and PDMS molds. Silicon wafer is used as the working substrate and Su-8 2000 series as the photo resist.

Early Preparation:

The first step is the selection of Su-8 photo resist as it depends on the desired channel height. The viscosity of Su-8 photo resist depends on the solvent, which in turn determines its spin coating thickness. The Su-8 photo resist along with height range are shown in Table 3.1:

Table 3.1: Different Su-8 photo resist along with height range

Su-8 photo resist	Desired height (µm)
Su-8 2005	5-8
Su-8 2015	15-40
Su-8 2025	25-80
Su-8 2075	75-180

Su-8 2005 is used for depositing the adhesion layer and Su-8 2075 is used for depositing 150 µm thick layer. Su-8 is poured into the tubes long time before fabrication to ensure dissolution of any bubbles formed during pouring. Any remaining bubbles are dissolved by blowing air through them.

Same Day Preparation:

Three hotplates: 195ºC, 95ºC and 65ºC are switched on and made to reach steady state temperature. Then the UV exposure system along with the UV lamp is started. The fabrication area should be very clean as dust particles can be a cause of defect during the soft bake. So the area around the spin coater and hot plates is thoroughly wiped clean before starting the fabrication.

Start of Fabrication:

Dehydration Bake:

Dehydration bake is done to remove moisture from the surface of the silicon wafer. This is done as Su-8 does not adhere well to damp or unclean surfaces. The wafer is put for 10 minutes at 195ºC, followed by 10 minutes cool down on a glass surface such as a Petri dish. If the wafer is put on a plastic surface it will melt. Then, a blast of nitrogen is provided to remove any dust or dirt that may have accumulated on the wafer.

Spin Coating of adhesion layer- Su 2005, 5µm thick:

Silicon wafer is placed on spin chuck of the spin coater (Figure 3.3) and aligned with the centering tool.

The following recipe is followed for the spin coating:

1. 0-500 rpm @ 100 rpm/s and hold for 35s while dispensing is performed
2. 500-2300 rpm @ 300 rpm/s and hold for 30s.

Su-8 2005 is deposited from the bottle while the wafer is spinning at 500 rpm. It is ensured that it is deposited directly in the middle of the wafer. Typically, the largest amounts of defects occur during spin coating which include small craters, dips, waviness or streaking. These defects are mainly attributed to particles or bubbles trapped in the Su-8 while spin coating. So this is a crucial step in the channel fabrication and requires much skill.

Soft Bake:

This process removes the solvent from the Su-8 and solidifies it so that it does not stick to the mask having channel design printed on it. In this process, the wafer is placed for 1 minute at 65 ºC, 2 minute at 95ºC, 1 minute at 65ºC again for a slower cool down and then finally cool down on glass surface for 10 minutes. Slower cool downs are better to reduce any thermal contraction.

Exposure:

The UV exposure system (Figure 3.4) cross-links the material by creating a chemical reaction in the exposed regions of the Su-8. Areas that are not exposed will dissolve away by the developer. It is important to select the right exposure dose for the given thickness of Su-8. If the dose is too low, it will cause the Su-8 features to lift off since the cross-linking will not extend down to the substrate and if it is too high, it will create features much larger than the mask. For 5 µm of Su-8 2005 thickness, the exposure dose is selected as 19258 mJ/cm^2. The wafer is then placed in the chamber and UV exposure is activated.

Post-Exposure Bake:

This process completes the cross-linking. After this procedure the exposed regions become visible. The wafer is placed for 1-2 minutes at 65ºC, 2-3 minutes at 95ºC, 1 minute at 65ºC again followed by cool down on glass surface for 10 minutes.

Spin Coating of first layer- Su-8 2075, 85µm thick:

Silicon wafer is placed on spin chuck and aligned with the centering tool.

The following recipe is followed for the spin coating:

1. 0-500 rpm @ 100 rpm/s and hold for 35s while dispensing is performed
2. 500-2250 @ 300 rpm/s and hold for 35s.

Soft Bake:

For the soft bake of the first Su-8 2075 layer, the wafer is placed for 6 minutes at 65ºC, 20 minutes at 95ºC, 3 minutes at 65ºC for a slower cool down and then finally cool down on glass surface for 10 minutes.

Figure 3.3: Spin coating equipment.

Figure 3.4: UV Exposure system

Spin Coating of second layer- Su 2075, 85 µm thick:

Silicon wafer is placed on spin chuck and aligned with the centering tool.

The following recipe is used for the spin coating:

1. 0-500 rpm @ 100 rpm/s and hold for 35s while dispensing is performed
2. 500-2250 rpm @ 300 rpm/s and hold for 35s.

Soft Bake:

The procedure for soft bake of the second layer is placing the wafer for 6 minutes at 65ºC , 20 minutes at 95ºC, 5 minutes at 65ºC for a slower cool down and then finally cool down on a glass surface for 20 minutes.

Exposure:

The wafer is placed in the mask aligner. The mask (Figure 3.5) is placed with printed side down on the wafer. Placing the mask in the wrong manner results in the channel features being jagged and ill defined. Then a vacuum pressure of 5 in Hg is applied. The vacuum performs the function of reducing the gap between the mask and Su-8 which reduces diffraction of light. The vacuum can be easily triggered by lifting the mask aligner lid. The dose of UV used for exposure is 60000 mJ/cm^2. Then the UV exposure is activated which completes the exposure.

Post-Exposure Bake:

The post-exposure baking procedure includes placing the wafer for 7 minutes at 65ºC, 15 minutes at 95ºC, 1 minute at 65ºC and then finally cool down on glass surface for 20 minutes.

Development:

The development jar is set up by filling it with the Su-8 developer. The nitrogen bubbling rod is placed in the solution and turned on very slowly until there is a little agitation. The wafer is placed in the wafer dipping holder and suspended in the jar with the long glass tube for 16 minutes. This is followed by washing with Isopropanol. If no white solute appears then all of the non cross-linked Su-8 has been developed. If not, then wafer is returned to the solution for another 30 seconds and the procedure is to be repeated. Finally, the wafer is washed with Ultra Pure water and dried with blown air (Figure 3.6).

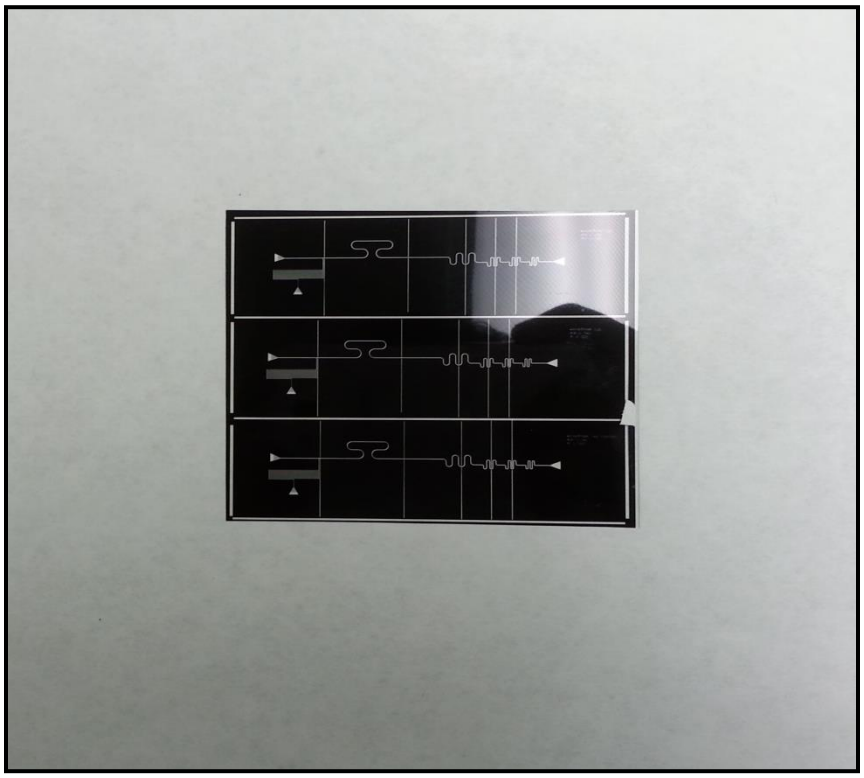

Figure 3.5: Mask with channel design

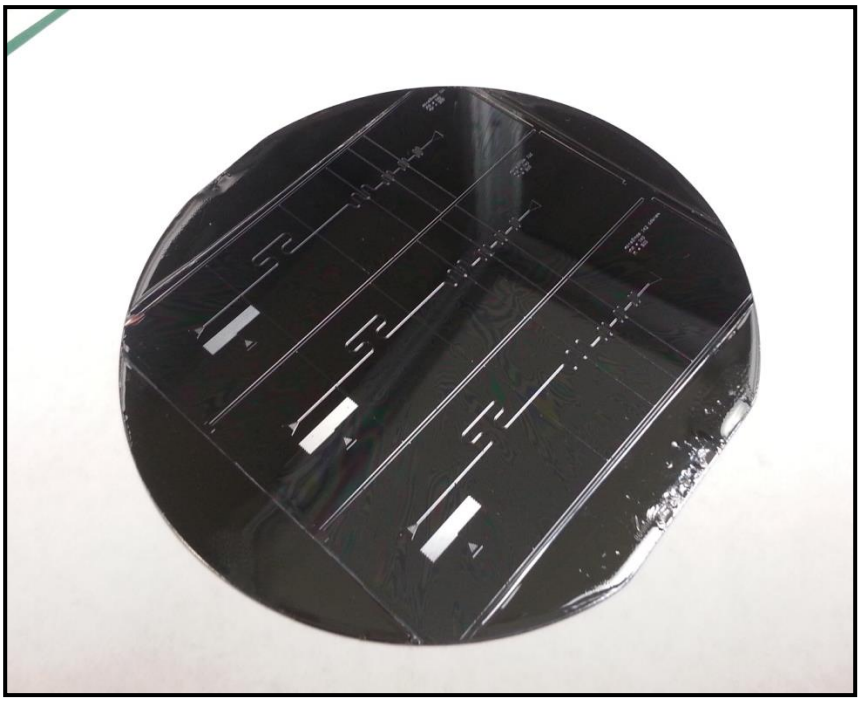

Figure 3.6: Master obtained after development

PDMS Molds:

PDMS replica molds are made from the master and then bonded to a glass microscope slide to create a microfluidic chip. For silicon wafer masters, the wafer is placed inside an aluminum weighing dish and the sides of the aluminum dish are curled in order to increase the PDMS holding capacity. The PDMS base and curing agent are mixed together into a 10:1 ratio by weight in a small plastic container. Lower ratios such as 5:1 will create a harder PDMS while higher ratios will create a softer PDMS. 4 grams of curing agent is mixed with 40 grams of PDMS base in a small plastic container. Mixing of curing agent and PDMS base will trap bubbles in the PDMS that must be removed. To remove the bubbles, the container is placed in the vacuum oven (20-25 psi) for 20 minutes. Then, the container is removed and the PDMS is poured over the master. After all of the bubbles are gone, the PDMS mold is placed on the hot plate at 95ºC for 1.5 hours (Figure 3.7). Once the PDMS mold is cured, it is removed from the hot plate and left to cool at room temperature. A scalpel is used to cut the mold and master away from the aluminum dish. Slowly the PDMS is trimmed away from the silicon wafer from the bottom. Once this is done the PDMS is peeled off slowly. The excess PDMS is trimmed off using the scalpel and cut into the desired shapes to get the microfluidic chips. The leather punch is used to punch the reservoirs into the PDMS. The punch should start on the design side of the PDMS to insure it is placed in the right spot. This is followed by blowing compressed air to blow off the tiny pieces of PDMS that remain in the reservoir and cleaning the PDMS with acetone, water and then blown with nitrogen.

Figure 3.8: PDMS mold on 95ºC hot plate.

PDMS Bonding:

To create a microfluidic chip from the PDMS mold, the mold is bonded to a glass slide. PDMS is spin coated on the glass slide as well to ensure uniform PDMS surface along the micro-channel surface inside the chip. The glass slide and the PDMS mold are placed into Plasma cleaner (PDC 001, Harrick Plasma) to create a permanent bond (Figure 3.9). The pump is turned on and the chamber is evacuated. Oxygen is released into the chamber for 15 seconds, followed by making the pressure inside the chamber to 500 millitorr (vacuum). The pump is turned off and the Plasma power is turned to 'high' for 8 seconds. Then, air is released into the chamber and the glass slide and PDMS mold are taken out and quickly put in contact. To ensure a good bond, the PDMS is lightly pinched at the sides until the entire PDMS is sealed. Then it is baked on hot plate at 95ºC for 1 hour. Then it is left on hot plate at 195ºC for at least 1 day to have good wetting properties in the channel. After completion of all the steps, a complete microfluidic chip is obtained (Figure 3.10).

Figure 3.9: Plasma Cleaner

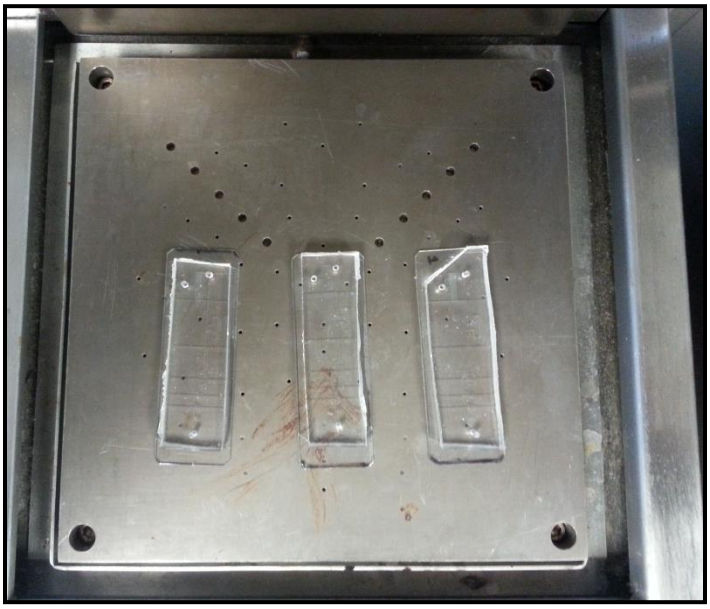

Figure 3.10: Three microfluidic chips obtained corresponding to the three same channel designs on the mask

Chapter 4: Chemicals and Interfacial tension

4.1 Chemicals

Silicone oil (10cSt, Sigma Aldrich) is used as the continuous phase and water-glycerol solution is used as the dispersed phase. The water-glycerol solution is prepared as 52% by weight of glycerol to nearly match the refractive index of Silicone oil and PDMS. Table 4.1 shows the physical properties of the continuous and the dispersed phase. Polystyrene fluorescent particles (Fluospheres 535/573, Invitrogen) having diameter of 1 µm are added to the dispersed phase with a concentration of 0.03% v/v. Fluorescent particles having diameter of 0.2 µm were also tried for this study. The aim for using smaller tracer particles was to improve the accuracy of the µ-PIV measurements (reducing interrogation area from 32*32 to 16*16). However, with our µ-PIV system, 0.2 µm tracer particles could not be distinctively observed in the acquired images (Figure 4.1), even at very low concentrations of tracer particles in the water-glycerol solution. This resulted in inaccurate and unreliable velocity vectors, which led to the use of 1 µm particles for this study. For the part where effect of surfactant is studied, two surfactants – Sodium dodecyl sulfate (SDS, Sigma Aldrich) and Tween 20 (Sigma Aldrich) are added to the dispersed phase in different concentrations. Wash Acetone and Isopropanol are used as the solvents for

different cleaning requirements during various stages of channel preparation and performing experiments.

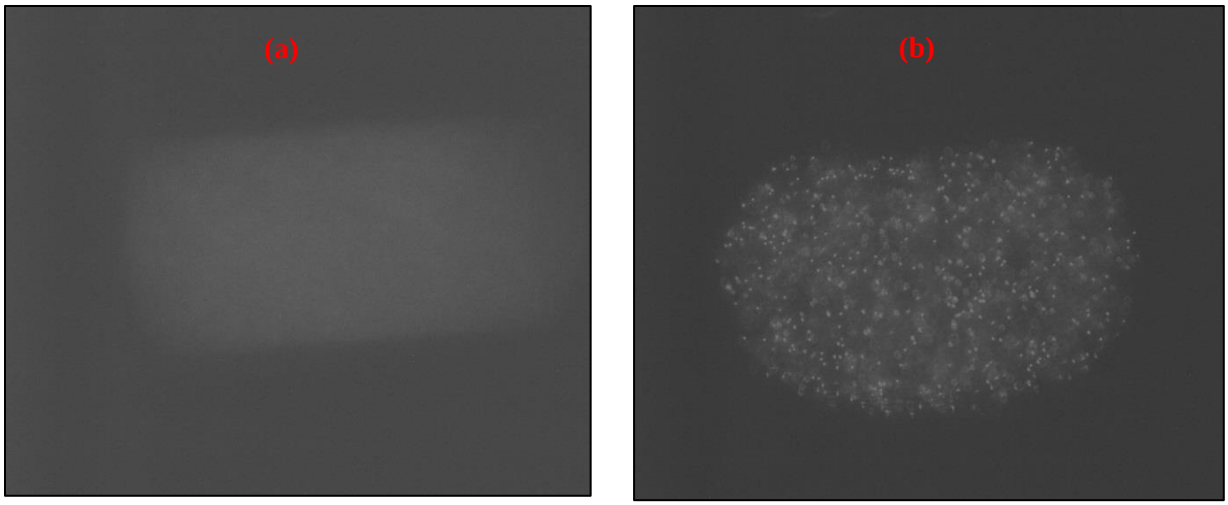

Figure 4.1: Acquired image of droplet with (a) 0.2 µm particles (b) 1 µm particles

Table 4.1: Physical properties of the continuous and the dispersed phase.

Phase	Density (kg/m^3)	Viscosity (mPa.s)	Refractive index
Continuous	930	10	1.399
Dispersed	1120.2	6.41	1.395

4.2 Interfacial tension

The interfacial tension between the continuous phase and the dispersed phase for different concentrations of SDS is found using the Wilhelmy Plate tensiometer. The interfacial tension for no addition of SDS is found to be 33.2 mN/m. The Critical micelle concentration (CMC) of SDS

in the water-glycerol solution is reported to be 11.3 mM [68].The concentration for below CMC condition for SDS is taken to be 0.466 mM and the corresponding interfacial tension is measured as 21.9 mN/m. The interfacial tension for above CMC condition is measured to be 10.515 mN/m. Pendant drop method is employed to find the CMC value of Tween 20 in water-glycerol mixture. The principle of this method is to estimate the interfacial tension between two immiscible liquids by formation of a drop of one liquid in another liquid. This image of the drop is then acquired through a camera, which is further processed by the software to get the value of interfacial tension.

The CMC of Tween 20 in water glycerol mixture was expected to be between 0.4-1mM. Several samples with varying concentration of Tween 20, ranging from 0.125 to 5.4mM are prepared in water glycerol mixture. The aim is to obtain the interfacial tension of each sample in Silicone oil. Initially, this posed a problem in getting a high phase contrast image of each sample drop as the refractive index of each sample is nearly same as that of Silicone oil. This problem was removed by adding fluorescent particles to each sample. It is shown that these particles have no effect on the interfacial tension between the sample and the Silicone oil.

For each concentration of Tween 20, the interfacial tension was measured for 30 minutes and repeated three times. The trend between interfacial tension and time is shown in Figure 4.2. Then, the interfacial tension was plotted against the inverse square root of late time (the time for which the interfacial tension reaches a steady state). This showed a linear trend and the value of equilibrium interfacial tension was found by taking the intercept of the line with the y-axis (i.e. at infinite time). The trend is shown in Figure 4.3. This methodology was performed for all samples and the value of interfacial tension was obtained for different concentrations of Tween 20. The final plot obtained is shown in Figure 4.5.

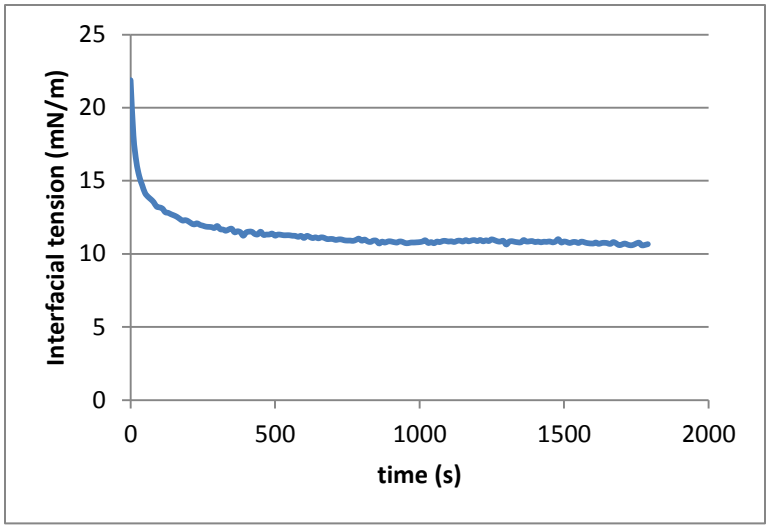

Figure 4.2: Trend between Interfacial tension and time

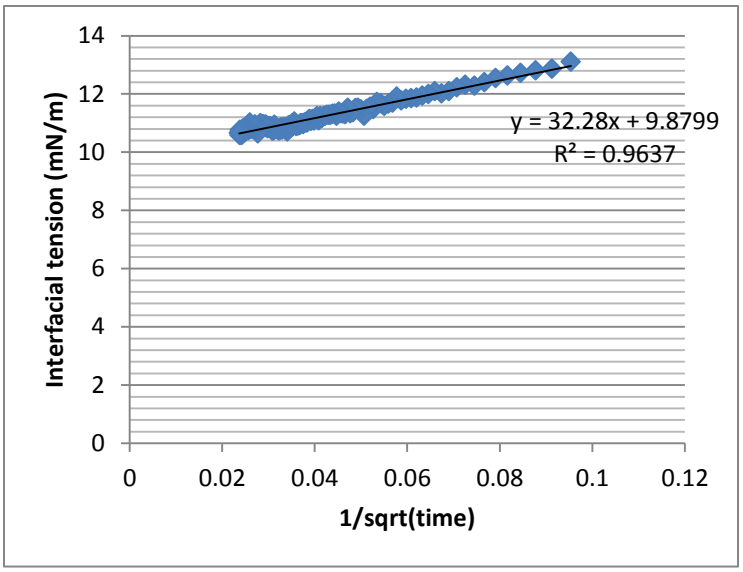

Figure 4.3: Trend between Interfacial tension and inverse square root of time

CMC is defined as a point on this plot where a sharp change in the slope should occur. To determine that point, the data points are divided into two separate regions and linear trends are plotted for these data points, as shown in Figure 4.4 .The intersection of these two lines gives us the value of CMC as 0.6mM. The value of CMC of Tween 20 in pure water is reported as 0.06mM. So, the addition of glycerol marks a 10 time increase in the value of CMC of Tween 20.

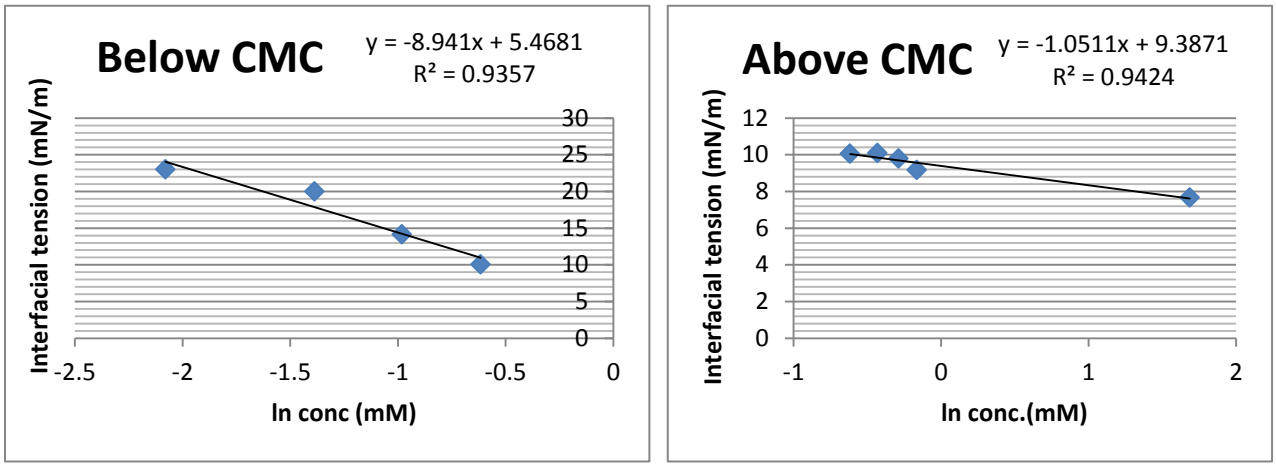

Figure 4.4: Linear trends for below and above CMC

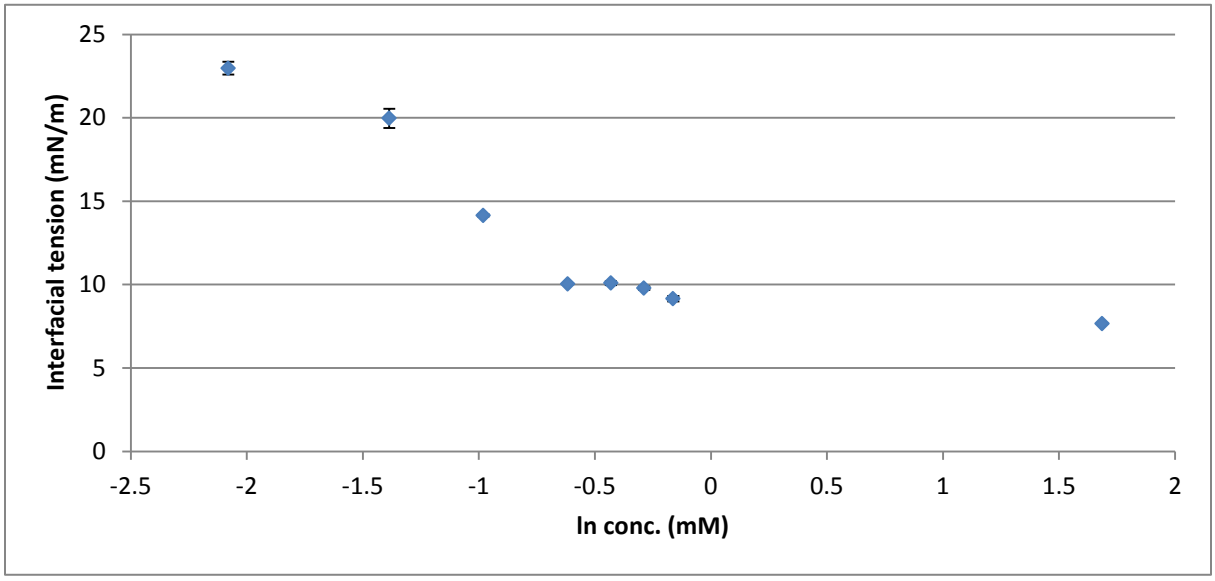

Figure 4.5: Plot of Interfacial concentration vs ln conc.

The concentration of Tween 20 for below CMC condition is taken as 0.165 mM and the corresponding interfacial tension is measured as 21.6 mN/m. The interfacial tension for 2X, 5X and 10X CMC is taken as 9.2 mN/m, 8.2 mN/m and 7.5 mN/m respectively.

There was an interesting observation on using higher concentration of SDS with the fluorescent particles. It was observed that increasing the SDS concentration to higher values (5 and 10X CMC) led to the aggregation of particles inside the droplet (Figure 4.6).

There were several possibilities associated with the aggregation of particles at higher concentration, like hydrophobic interactions between the particles and aggregation due to the presence of high electrolyte concentration. Some of the remedies tried to resolve the aggregation problem was diluting the microsphere suspension to reduce electrolyte concentration and adjusting the pH of the solution [69]. The particles are stable from pH range 6-12, but pH measurement of samples with increasing SDS concentration revealed that the pH of 2X CMC solution is 6.84, which eventually decreases to 5.50 for 10X CMC solution. Increasing the pH of 10X CMC solution to 7.2 using MOPS buffer (pH 7.2, 2mM) also did not resolve the aggregation problem. Finally, using fresh stock of SDS, combined with partial heating along with longer sonication resolved the aggregation problem significantly. It is recommended that the use of same surfactant solutions for prolonged period of time should be avoided and fresh samples should be prepared after regular intervals of time.

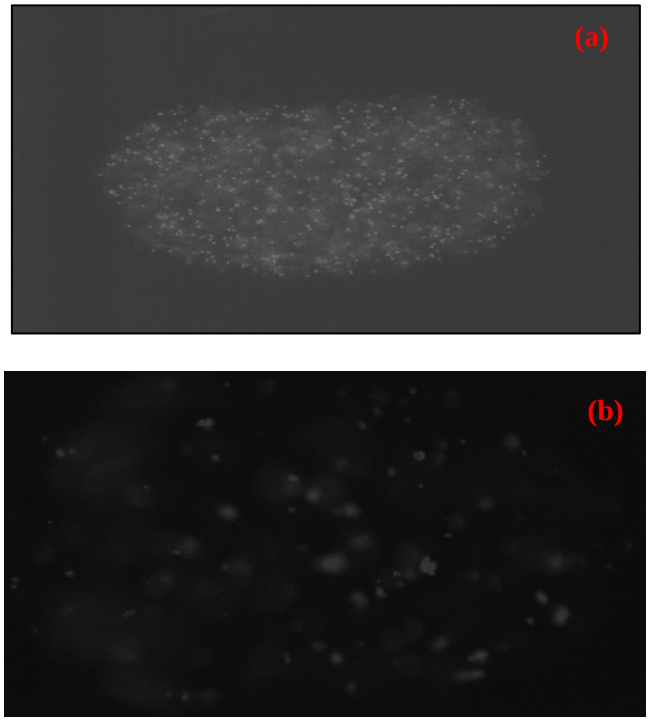

Figure 4.6: Image of droplet with (a) No SDS (b) SDS at 5X CMC

Chapter 5: Experimental system and Methodology

5.1 Experimental system

The experimental system (Figure 5.3) comprises of two sub-systems; droplet detection and triggering sub-system, and the µPIV sub-system. The experimental system is connected in such a manner that the droplet detection and triggering sub-system acts as an external actuator for the µPIV sub-system. The experimental system is developed by a previous PhD student, Zeyad Almutairi [24].

5.1.1 Droplet detection and triggering sub-system

The droplet detection and triggering sub-system is based on optical detection of the droplets. Two light sources, Helium Neon laser (HeNe, 633 nm) and infra-red laser (IR, 780nm) are used in this sub-system. The HeNe laser is used to check the circularity of the fiber cross-section for optimum light intensity. The IR laser is used to detect the presence of droplets. Both single and multi-mode fibers are used for detecting the droplets (Figure 5.2). Light path along the aligned optical fibers gets distorted on the passage of a droplet. This light signal is sensed by a photomultiplier tube (PMT- H9656-02, Hamamatsu), which further gets converted to a voltage

signal. This is followed by the use of a voltage conditioning circuit, which conditions the voltage signal to remain in the signal limitations of the synchronizer (Figure 5.1).

5.1.2 µPIV sub-system

For the µPIV sub-system, Nikon Ti-Eclipse microscope is used to place the PDMS channel and guide the light from the source to the channel through a 20X objective. The depth of correlation of the system is found to be 12.75 µm [55]. A dual head laser (ESI – Nd:YAG) is used as the light source to illuminate the region of interest. The laser power is 15 mJ and emits light at a wavelength of 532 nm. The laser can operate with a frequency of 15 Hz. A dual frame 1.4 Mega Pixel (1344 × 1024 pixel^2) CCD camera (Hamamatsu C8484-05CP) is used for the acquisition of droplet images. The camera can acquire images with a frequency of 12.2 Hz. A MotionPro (IDT Vision) Timing hub is used to synchronize the illumination of the field of view by the Nd:YAG laser and acquisition of the image by the CCD camera. Eight channels can be synchronized by the Timing hub. Dynamic Studio (V2.3, Dantec Dynamics) is used to control the settings like time difference between the two pulses, internal or external triggering etc. Dynamic Studio is also used for the post-processing of the acquired sets of image data [24].

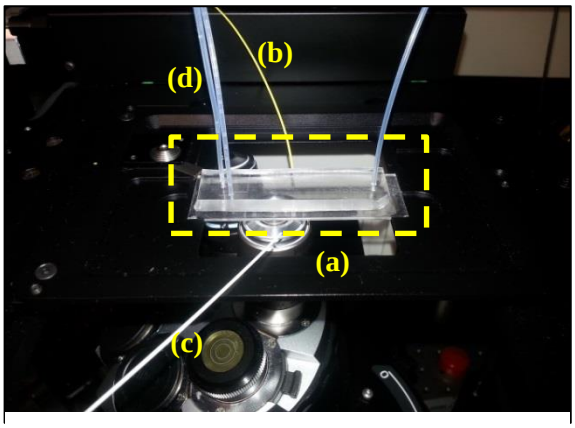

Figure 5.2: Close-up of the PDMS microchannel with fibers (a) PDMS microchannel (b) single mode fiber (c) multi-mode fiber (d) Teflon tubing for fluid pumping

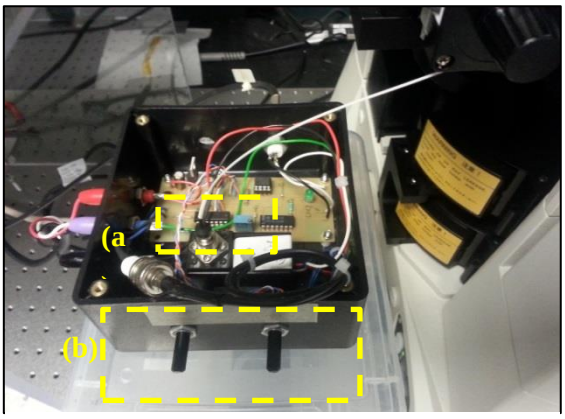

Figure 5.1: Close up of the triggering circuit (a) Photomultiplier tube (b) sensitivity and trigger level of the circuit

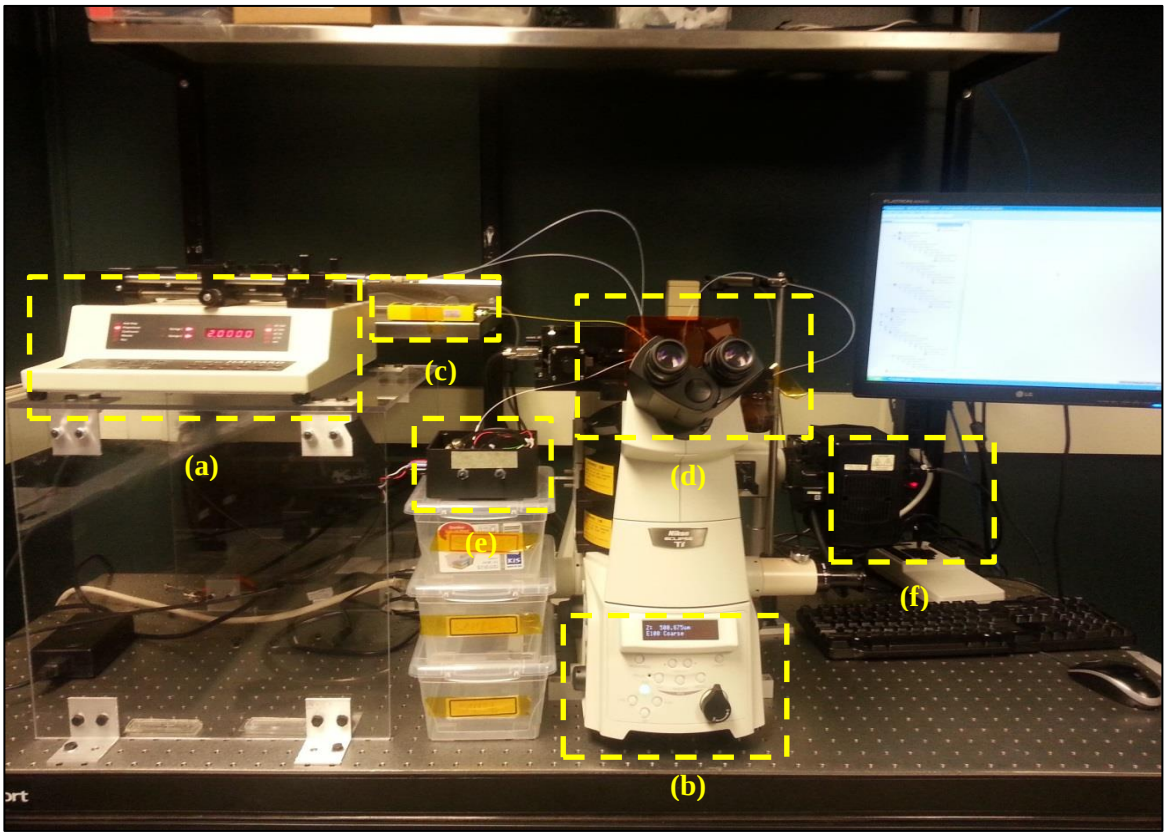

Figure 5.3: The experimental setup for the study. (a) Syringe pump (Pump 33, Harvard Apparatus); (b) Nikon Ti-Eclipse microscope; (c) IR laser (d) PDMS microchannel with fibers (e) triggering circuit (f) input for Nd:YAG laser

5.2 Methodology

The methodology followed for the experiments and subsequent analysis is described next. A high precision Syringe pump (Pump 33, Harvard Apparatus) is used to pump the fluids into the micro-channel. Glass syringes along with Teflon tubings are used for the pumping of the fluid. The diameter of the syringes is chosen corresponding to the flow rates so that the resulting flow from the syringe pump is stable. The glass syringes are thoroughly cleaned with wash acetone, isopropanol and rinsed with water before their use in the experiments. The PDMS channel is primed with Silicone oil for 30 minutes to ensure complete wettability of the channel walls to the oil. Then the dispersed phase is introduced from the branching channel at the T-junction and droplets are generated, which move downstream along the continuous phase. The flow rate for the dispersed phase is kept to be at 20% of the continuous phase. This ratio is selected so that small droplets are formed which can be observed in the field of view of the camera. This droplet flow is made to run for at least 30 minutes so that the flow rates from the syringe pump have stabilized and result in uniform sized and equally spaced droplets. In the meantime, single mode and multi-mode fibers are inserted into the waveguides and positioned at the extreme ends of the waveguide close to the channel. Extreme caution is taken while inserting the fibers as they are extremely fragile and minor damage to the fibers makes the entire microfluidic chip redundant. The single mode fiber is connected to the IR laser, while the multi-mode fiber is connected to the triggering circuit. The droplets are detected using the optical detection system, as discussed in Section 5.1.1. The crucial part in this study is to detect the droplets at the same channel location every time. This condition is referred to as the phase locking of the droplets and is achieved by manually adjusting the triggering circuit. The variables used to adjust the external trigger are the

sensitivity of the PMT, the triggering level of the circuit and the intensity of the IR laser. This is a very crucial part during the experiments and success with the tuning of the triggering circuit ensures that the droplets are detected at the same location in the channel.

The most important factors which affect the phase locking of the droplets are the light quality through the fibers and uniform droplet generation rate and size. There are several contributing factors to achieve optimum light quality through the fibers, like fiber cross-section, waveguide shape and fiber alignment. A Soft Strip (Micro Electronics Inc.) is used to strip the fiber jacket to its cladding diameter of 125 µm and a cleaver (FI-6000, Fiber Instrument Sales Inc.) is used to cut the fiber precisely normal to the cross section. In this way, the fiber achieves a completely circular cross section and passes light straight-on without any deflection. Also, it has been observed that the waveguide having straight ends rather than curved ends enhance achievement of phase-locking. To improve the fiber alignment, the waveguide width is decreased to 135 µm and weights are placed on the fibers to remove any height misalignment between the fibers. To achieve uniform droplet generation rate and size, proper wetting of PDMS channel by the silicone oil is important. Improper wetting properties in the PDMS channel might get induced due to poor Plasma treatment. Some combinations of process gases and sample materials may generate particulates and contaminants, which accumulate on the chamber wall. Over time, these contaminants may decrease the plasma power and effectiveness of the plasma process. The chamber may require cleaning to remove these contaminants, if a change to the plasma process or plasma intensity is detected. The plasma chamber is made of borosilicate glass (Pyrex) and may be cleaned using similar cleaning methods for standard laboratory glassware, such as:

1. Soaking or wiping the plasma chamber surface with acetone or isopropyl alcohol.
2. Cleaning the plasma chamber using a standard laboratory glassware cleaner (e.g. Alconox).

After cleaning the chamber, leave it for 2-3 days as it takes time to return to its normal operation [70]. Due consideration to the above discussed factors increase the chances of success with the phase-locking of the droplets. Once phase-locking is achieved, the acquisition of droplet image is done using Nd:YAG laser as the illuminating source and the CCD Hamamatsu camera for capturing the images. For the complete study, all image acquisitions have been performed at the depth-wise middle plane of the channel i.e. z/h =0.5. A schematic illustration of the experimental system is shown in Figure 5.4.

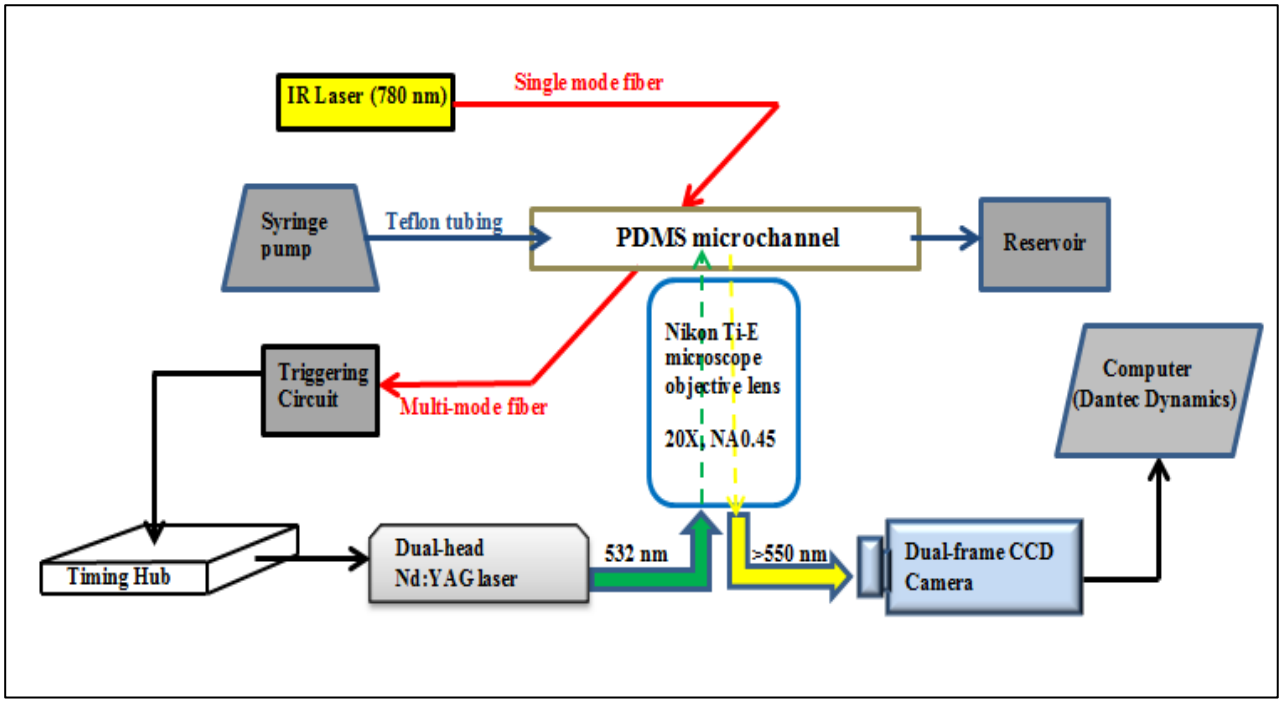

Figure 5.4: A schematic illustration of the experimental system

Table 5.1, Table 5.2 and Table 5.3 show the flow rate and the mean velocity of the continuous phase used in the experiments for SDS and Tween 20:

Table 5.1: Flow rate of the continuous phase for different concentration of SDS at the squeezing regime (Ca=0.001)

SDS concentration	Interfacial tension (mN/m)	Qc (ul/min.)	Mean velocity(m/s) (U_m)
Nil	33.2	6.25	0.0035
Below CMC	21.9	4.15	0.0023
2X CMC	10.515	2	0.0011
5X CMC	10.515	2	0.0011
10X CMC	10.515	2	0.0011

Table 5.2: Flow rate of the continuous phase for different concentration of SDS at the transition regime (Ca=0.005)

SDS concentration	Interfacial tension (mN/m)	Qc (ul/min.)	Mean velocity(m/s) (U_m)
Nil	33.2	31.3	0.017
Below CMC	21.9	20.75	0.0115
2X CMC	10.515	10	0.0056
5X CMC	10.515	10	0.0056
10X CMC	10.515	10	0.0056

Table 5.3: Flow rate of the continuous phase for different concentration of Tween 20 at the squeezing regime (Ca=0.001)

Tween 20 concentration	Interfacial tension (mN/m)	Qc (ul/min.)	Mean velocity(m/s) (U_m)
Below CMC	21.6	4.09	0.0023
2X CMC	9.2	1.74	0.0009
5X CMC	8.2	1.55	0.0008
10X CMC	7.5	1.42	0.0007

5.3 PIV Analysis

Around 100 images of droplets (in pairs) are acquired corresponding to each set of image acquisition of droplets. The time difference between the two successive images in a pair is chosen in such a way that the displacement of particles between these two images is nearly 2-4 pixels. Consequently, the analysis of the acquired image pairs using Dynamic Studio (v2.3, Dantec Dynamics) is performed to obtain the velocity patterns inside the droplet. Initially, the adaptive correlation with an interrogation area of 32*32 is done for each image pair of the droplet. This is followed by moving average validation, Peak validation (relative to peak 2: 1.02) and application of a coherence filter (radius-15 pixels) to filter out any remaining outliers. Then, the statistical average of the data processed so far is performed using vector statistics. This provides us with the velocity vectors in the droplet. The analysis scheme is shown in Figure 5.5. The velocity vectors are an indicator of the flow direction and velocity magnitude in different regions inside the droplet. The velocity vectors at some regions have two components: u in the x-direction and v in the y-direction.

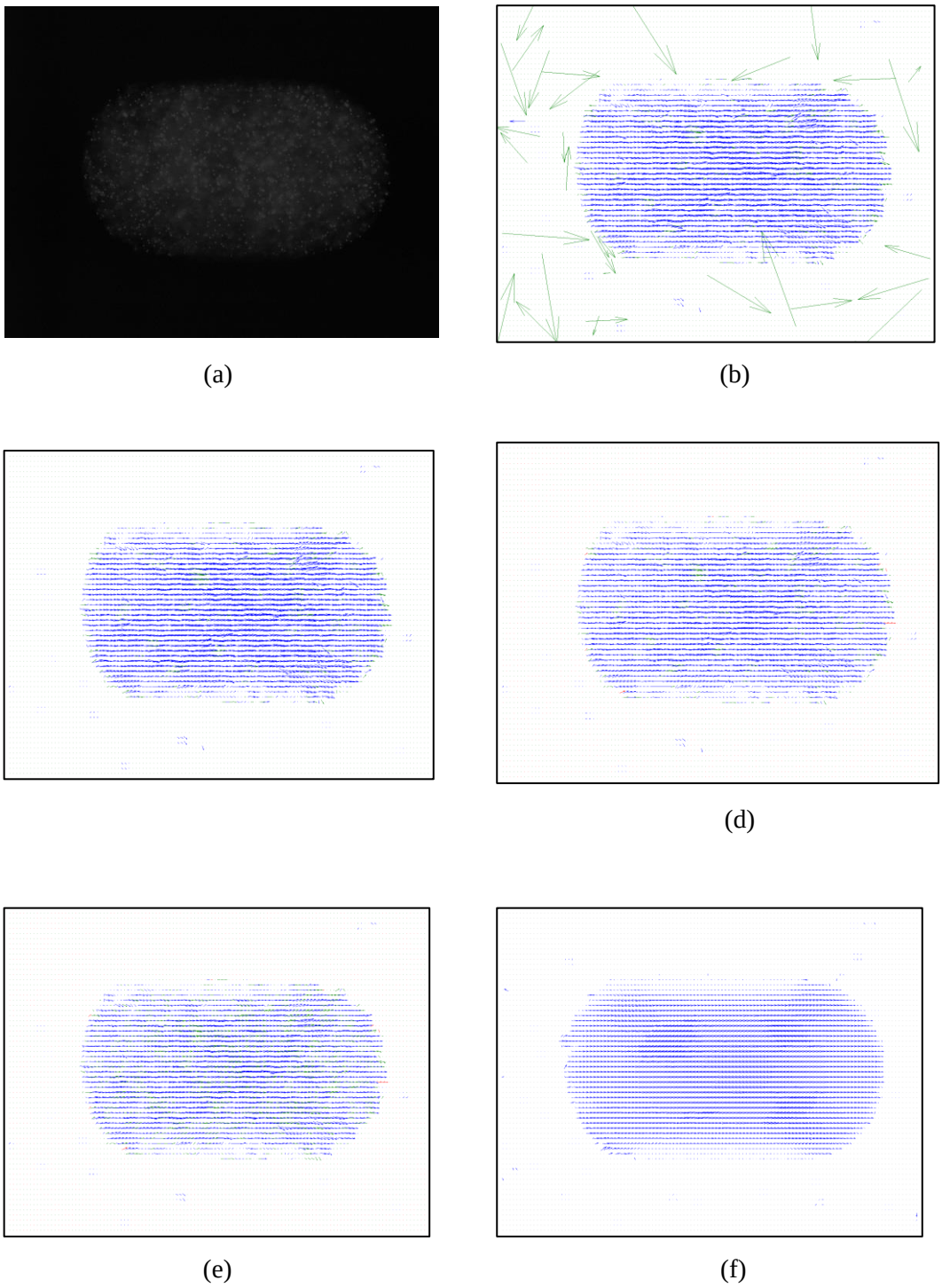

Figure 5.5: PIV Analysis scheme (a) acquired image of droplet (b) Adaptive correlation (c) Moving average validation (d) Peak validation (e) Coherence filter (f) Vector Statistics

Then, the net magnitude of the velocity, V can be calculated using equation

$$V = \sqrt{u^2 + v^2} \tag{5.1}$$

Further subtraction of the actual mean velocity from the velocity vectors results in the internal flow fields inside the droplet. The internal flow fields inside the slug droplet obtained after the analysis is shown in Figure 5.6. Two axi-symmetric vortices are mainly present inside the droplet, which produce a circulating flow inside the droplet. It should be noted that this flow field pattern is observed at the depth wise middle plane of the channel i.e. z/h = 0.5.

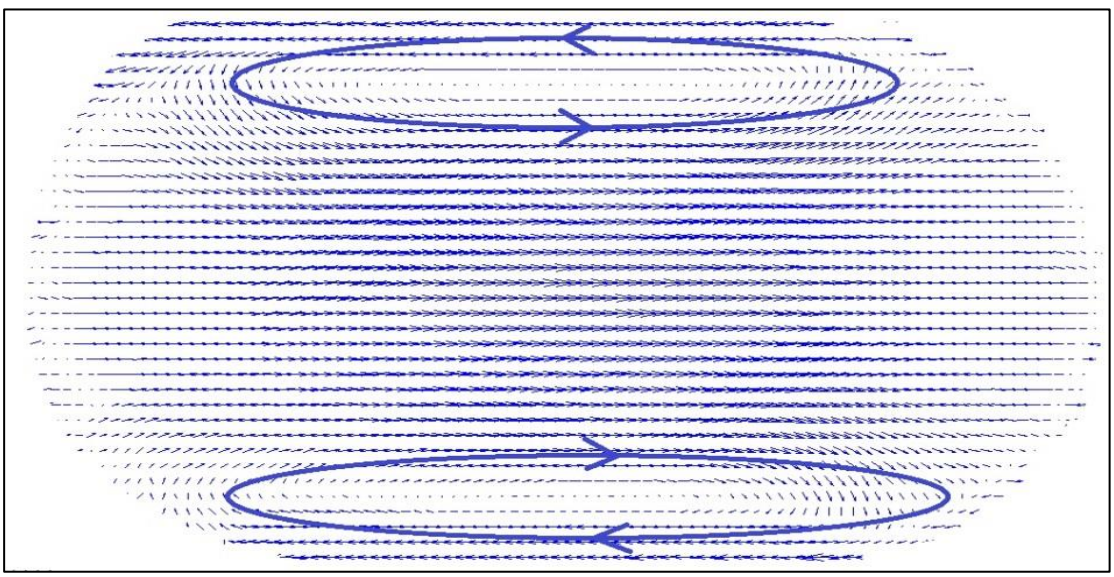

Figure 5.6: Internal flow fields inside the droplet, with the presence of two main vortices

Chapter 6: Effect of surfactant concentration on the internal flow

6.1 Introduction

The knowledge of internal flow fields inside a moving droplet is important in the area of droplet microfluidics. This is because the mixing efficiency of the reagents added to the droplets depends on the internal flow fields, which in turn affect the chemical reaction occurring inside the droplet. Numerous studies of flow fields inside droplets have been done with μPIV technique, both with and without surfactants [58,71,72]. Malsch et al. [58] reported that the flow fields inside the droplets are mainly induced due to friction at the interface, which has two contributing factors: liquid/wall friction and liquid/liquid friction. They showed that winding channels are more effective than linear channels to improve the mixing inside the moving droplets (Figure 6.1). This is attributed to the complex flow patterns produced inside the droplet moving in a winding channel as compared to the linear channel.

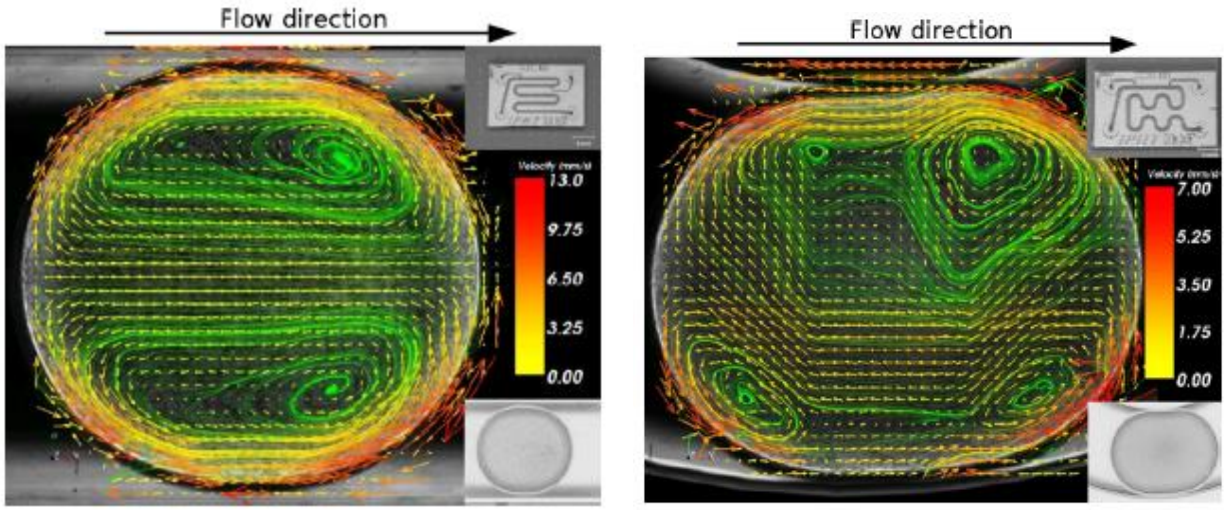

(a) (b)

Figure 6.1: Flow fields inside a moving droplet (a) Symmetrical flow fields are induced in linear micro-channel (b) Complex internal flow is induced in droplet moving in winding microchannel. Reprinted from [58], with permission from Elsevier.

Several surfactant studies have been performed to understand interfacial retardation in a moving droplet [64,65,66]. They observed significant interfacial retardation at low surfactant concentrations. The remobilization of the internal flow at high surfactant concentration depends on the type of surfactant (size, exchange kinetics etc.)

Actual insight of surfactant effect on internal flow fields using µPIV technique is performed in this study. This study aims to observe the effect of surfactant concentration, droplet regime, surfactant size and droplet shape on the internal flow fields inside the droplet.

6.2 Experimental setup and Methodology

The experimental setup comprises of two sub-systems: droplet detection and triggering sub-system, and the µPIV sub-system. Details about these assemblies were presented in Section 5.1. The experimental system is connected in such a manner that the droplet detection and triggering sub-system acts as an external actuator for the µPIV sub-system.

The microchannel designs used for the experiments are discussed in Section 3.1. Silicone oil is used as the continuous phase and water-glycerol mixture along with the 1 µm fluorescent particles is used as the dispersed phase. The water-glycerol solution comprises of 48% water and 52 % glycerol by weight. This composition is made so as to match the refractive index of the dispersed phase with that of the continuous phase. High precision syringe pump (Pump 33, Harvard Apparatus) is used to pump both the phases into the microchannel.

The methodology for conducting the experiments is described briefly. Silicone oil is made to flow in the microchannel for about 30 minutes prior to the introduction of the dispersed phase. This droplet flow is made to run for at least 30 minutes so that the flow rates from the syringe pump have stabilized, resulting in generation of uniform sized and equally spaced droplets. In the meantime, optical fibers are inserted and aligned in the waveguide. After the flow rates have stabilized, the triggering circuit is adjusted so as to achieve phase-locking of the droplets. This is a very tricky part and success with the tuning of the triggering circuit ensures that the droplets are detected at the same location in the channel. Once phase-locking is achieved, the acquisition of images is done at the depth-wise middle plane of the channel. The acquisition of about 100 image pairs is done such that the particle displacement is ~2-4 pixels in each pair of images.

Consequently, the analysis of the acquired images is performed to obtain the velocity vectors inside the droplet.

6.3 Secondary Analysis of the Velocity Profile

Vorticity at a point is defined as the local rotation or curl of the velocity field. The knowledge of the vorticity distribution inside the droplet helps in identifying the location and intensity of the circulation zones inside the droplet. This is a relevant parameter to quantify the internal flow as any change in the internal circulating flow of a droplet would correspond to a change in the vorticity of the circulation zones. After obtaining the velocity vectors from the PIV analysis, secondary analysis is performed to obtain the vorticity maps inside the droplet. Since the velocity vectors are in two-dimensions, the vorticity around the normal direction is computed as

$$\omega = \frac{\partial V}{\partial x} - \frac{\partial U}{\partial y} \tag{6.1}$$

where U and V are velocity vectors in the x- and y- axes respectively and ω is the vorticity along the z-direction. To compare the internal flow for different cases, vorticity is non-dimensionalized with respect to the channel width (W_c) and the mean velocity of the continuous phase (U_m).

6.4 Experimental results and discussion

6.4.1 Effect of SDS on internal flow in the squeezing regime (Ca=0.001)

The study of the effect of SDS on the internal flow inside the droplet is first performed in the squeezing regime (Ca = 0.001). The results for the vorticity inside the droplet with increasing concentration of SDS are shown in Figure 6.2.

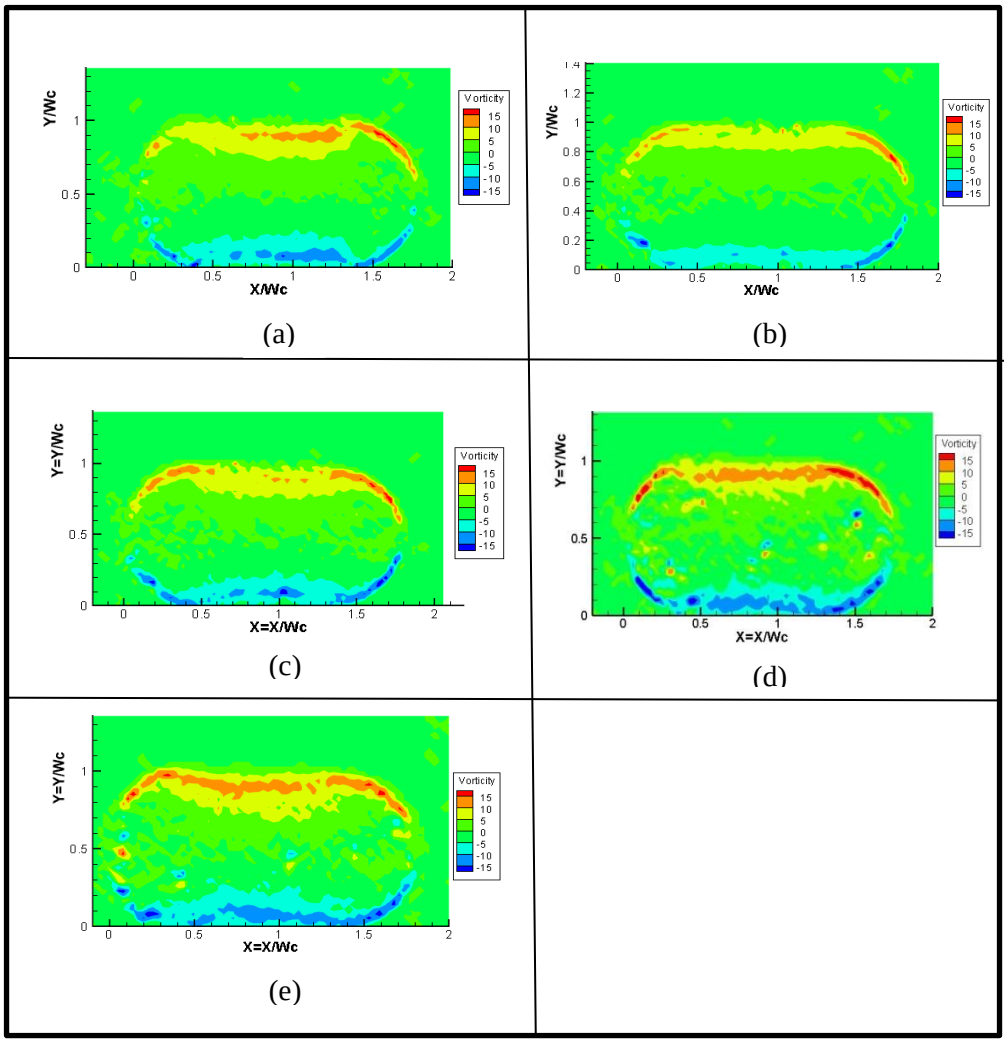

Figure 6.2: Vorticity map inside droplet with increasing SDS concentration at the squeezing regime (a) No SDS (b) Below CMC (c) 2X CMC (d) 5X CMC (e) 10X CMC

There are certain surfactant properties which affect the internal flow inside a droplet. These primarily include desorption rate, bulk concentration and micellar break up kinetics of the surfactant. The relative significance among these properties governs the surfactant behavior inside moving droplets. Whenever surfactant is present inside a moving droplet, it tends to adsorb at the stagnation points at the leading edge of the droplet. The surfactant monomers adsorbed at the interface here are then swept away by the internal circulating flow along the interface towards the trailing edge. At this end, the monomers tend to desorb and diffuse towards the bulk of the droplet.

For no SDS added to the dispersed phase, the vorticity map is symmetric as expected. Dimensionless vorticity in the range of 10-15 is present in the region of the two main vortices. Vortices of high intensity are present at the leading and trailing edge of the droplet due to the liquid-liquid interaction at the droplet interface. SDS is a smaller anionic surfactant and has a faster desorption rate as compared to a relatively bigger surfactant like Tween 20. This is because the work required to desorb a small surfactant molecule against surface pressure is less as compared to a bigger molecule [64]. As the concentration of SDS is increased to below CMC condition, retardation in the internal flow is observed. This can be seen from the decrease in the value of vorticity in the region of the two vortices. This can be attributed to the low concentration of SDS present inside the droplet. The bulk diffusive resistance is inversely proportional to the bulk concentration of the surfactant. Below CMC, the bulk concentration of SDS is less which results in high bulk diffusive resistance. The surfactant molecules are swept away from the leading edge towards the trailing edge of the droplet. Due to high bulk diffusive resistance, the monomers are not able to diffuse into the bulk and tend to accumulate at the trailing edge. This leads to a gradient in the surfactant concentration from the rear towards the

front of the droplet. This results in a high gradient in interfacial tension across the droplet, low interfacial tension at the trailing edge and high on the leading edge. The tendency of high tension liquid region to pull surrounding liquid towards it is responsible for the action of Marangoni forces on the droplet. These forces act opposite to the direction of internal interfacial flow. Hence, significant retardation is observed inside the droplet. As the concentration of SDS is further increased to 2X CMC, the bulk concentration of SDS inside the droplet is increased. This marks a decrease in the diffusive resistance inside the droplet, which leads to the accumulated surfactant getting diffused as compared to below CMC condition. In addition to monomers, micelles also appear which exist in exist in equilibrium with each other. This leads to lower gradients in interfacial tension, and subsequently, lower Marangoni stresses. The regions showing partial remobilization start appearing at 2X CMC, but still significant retardation is present inside the droplet. Increasing the SDS concentration to 5X CMC leads to a high bulk concentration of SDS inside the droplet. There are also micelles present at the leading edge sub-surface which act as monomer sources and prevent loss of monomer concentration here. On the trailing edge, negligible diffusive resistance prevents accumulation of monomers here. This results in maintaining a nearly uniform concentration of monomers along the interface, which indicates absence of any interfacial tension gradients and subsequently, absence of any Marangoni stresses on the droplet interface. This results in complete remobilization of the internal flow inside the droplet. Further increasing the concentration to 10X CMC results in similar observations. The internal flow is completely remobilized and is similar to the no-surfactant case. Since the flow remobilization in the droplet can be completely attributed to the removal of the Marangoni stresses at high concentration of SDS, the effect of intrinsic surface rheology is fairly taken to be negligible.

6.4.2 Effect of SDS on internal flow in the transition regime (Ca=0.005)

The study of the effect of SDS on the internal flow inside the droplet is secondly performed in the transition regime (Ca = 0.005). The changing of the droplet regime from squeezing to transition increases the flow rate of the continuous and the dispersed phase. This results in an increase of convection rate inside the droplet due to the increase in velocity. So, the change of regime to transition would allow us to observe the effect of SDS on the internal flow at increased convection rate inside the droplet. The results for the vorticity inside the droplet with increasing concentration of SDS in the transition regime are shown in Figure 6.3.

For no SDS added to the dispersed phase, the vorticity map is symmetric as expected. Vorticity in the range of 10-15 is present in the region of the two main vortices. Vortices of high intensity are present at the leading and trailing edge of the droplet due to the liquid-liquid interaction at the droplet interface. Akin to the previous case, severe retardation is observed inside the droplet flow when the concentration of SDS is below CMC. This is attributed to the presence of high diffusive resistance at low SDS concentration. When the concentration of SDS is increased to 2X CMC and then to 5X CMC, the retardation inside the droplet flow is still prevalent and the internal flow is not completely remobilized. This can be attributed to the slow micellar break up kinetics of SDS at high concentration [26] as compared to the fast rate of convection present inside the droplet at this regime. The monomers adsorbed at the leading edge of the droplet are swept away faster by convection towards the trailing edge, than can be replenished by micelles present at the sub-surface region at the leading edge. This leads to a concentration gradient

getting developed along the droplet interface, which ultimately leads to the action of opposing Marangoni forces, which retards the internal flow.

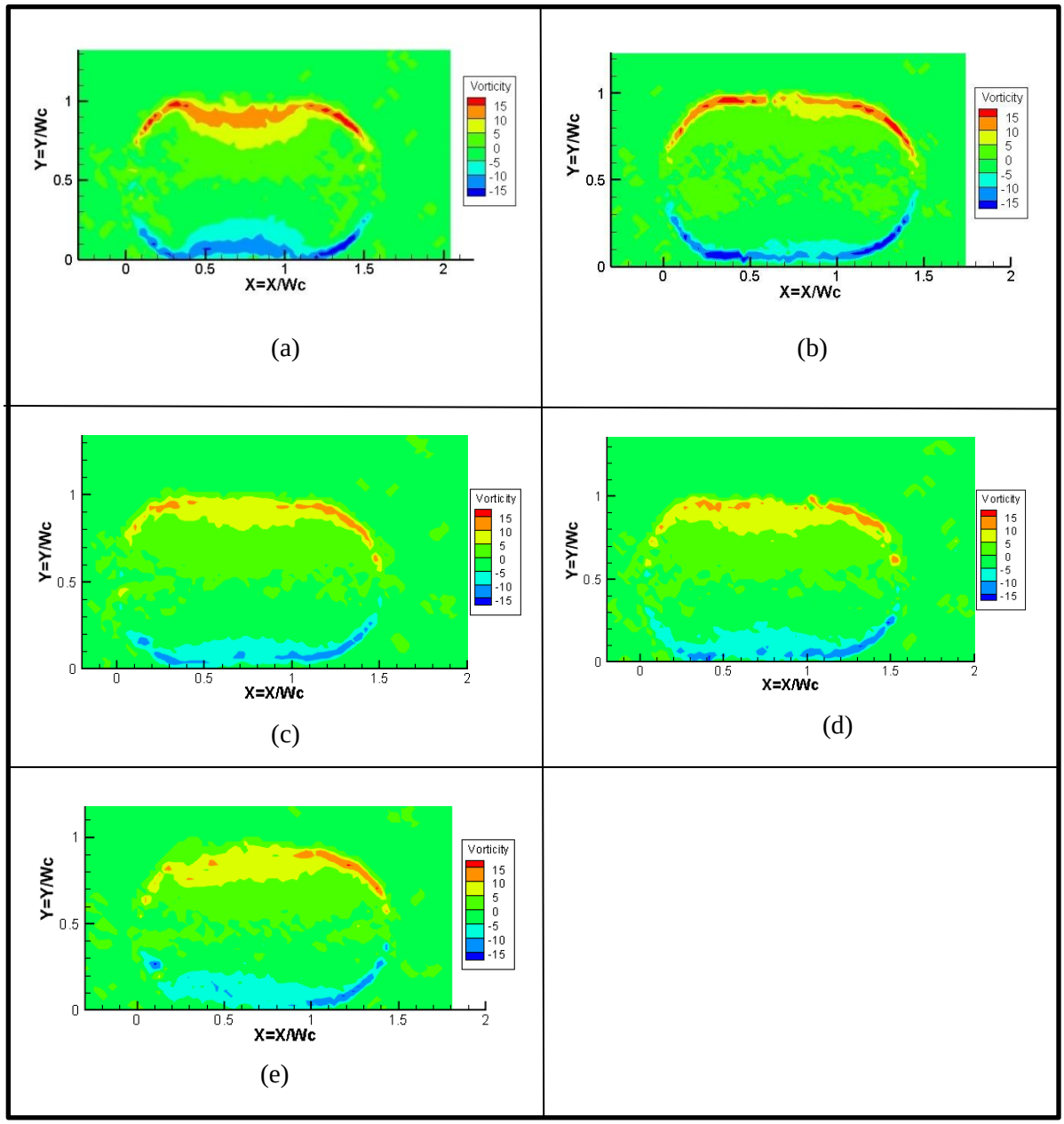

Figure 6.3: Vorticity map inside droplet with increasing SDS concentration at transition regime (a) No SDS (b) below CMC (c) 2X CMC (d) 5X CMC (e) 10X CMC

Further increasing the SDS concentration to 10X CMC does not results in remobilization of the internal flow, as was observed in the squeezing regime. Retardation is still present inside the droplet, even though the bulk concentration is very high. This is because the convective rate inside the droplet is faster than the rate at which micelles can replenish the monomers. So, even at very high bulk concentration of SDS, the internal flow inside the droplet remains retarded.

6.4.3 Effect of Tween 20 on internal flow in the squeezing regime (Ca = 0.001)

The effect of surfactant size on the internal flow is also studied. For this, another surfactant, Tween 20 is utilized to study the effect on the internal flow inside the droplet. The effect of increasing Tween 20 concentration is performed in the squeezing regime (Ca = 0.001). Tween 20 is chosen for this study as Tween 20 is a relatively larger surfactant as compared to SDS and their use allows a wide timescale of adsorption kinetics to be investigated [67]. The results for the vorticity inside the droplet with increasing concentration of Tween 20 at the squeezing regime are shown in Figure 6.4.

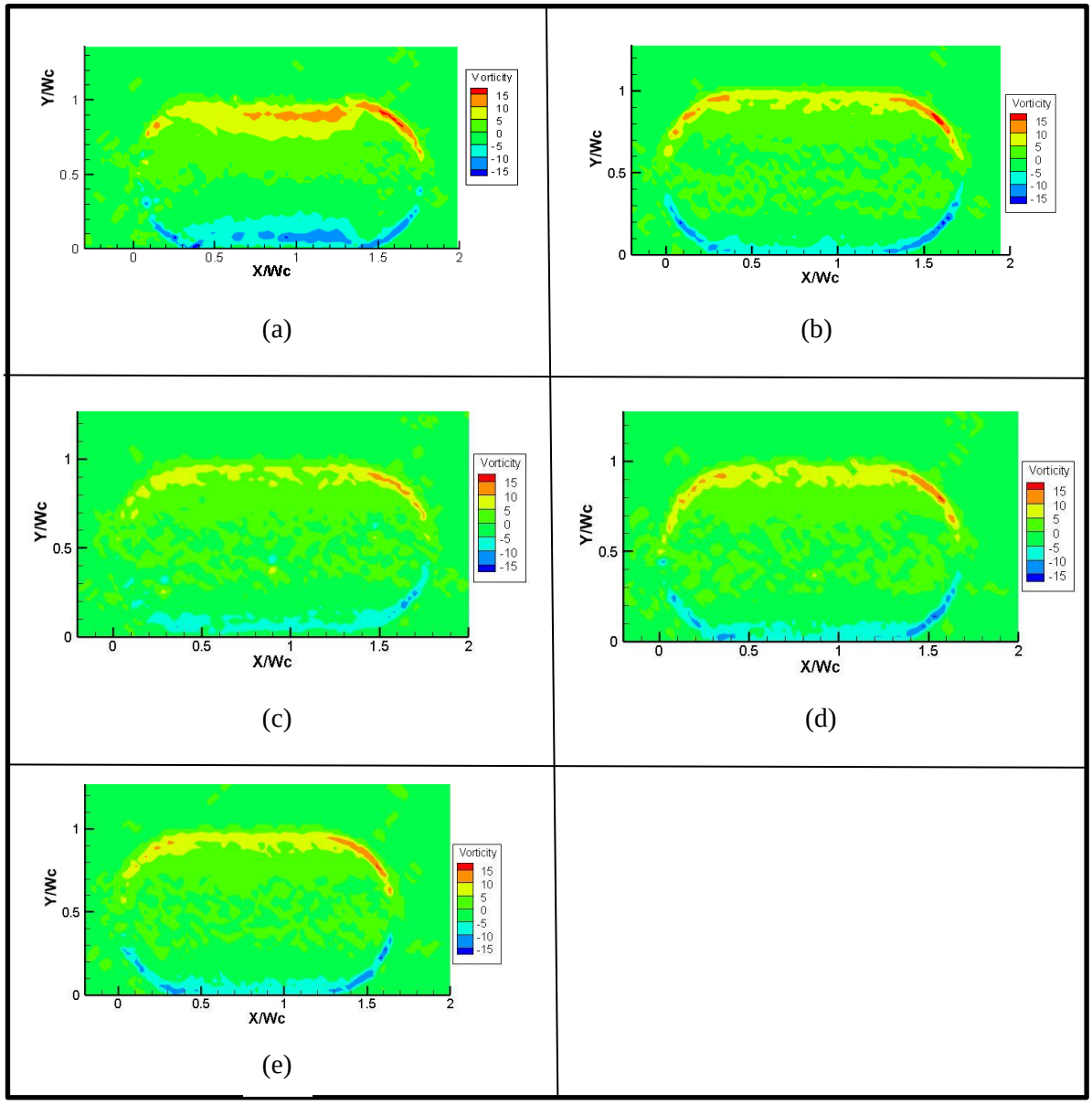

Figure 6.4: Vorticity map inside droplet with increasing Tween 20 concentration at squeezing regime (a) No Tween 20 (b) Below CMC (c) 2X CMC (d) 5X CMC (e) 10X CMC

Tween 20 is a bigger surfactant as compared to SDS. The work required against surface pressure to desorb a bigger molecule is higher as compared to a smaller molecule, resulting in slower desorption kinetics of Tween 20 as compared to SDS. Analogous to the previous results, internal flow retardation is observed at below CMC concentration of Tween 20. As the concentration is increased to 2X CMC, the retardation is still present due to the action of Marangoni forces. Eventually increasing the concentration to 5X and 10X CMC leads to a partial remobilization of the internal flow inside the droplet. This can be attributed to the decrease in the bulk diffusive resistance as the bulk concentration of Tween 20 is increased. Complete remobilization, as was observed for SDS, is not observed for Tween 20. This can be attributed to two reasons: slow desorption rate of Tween 20 and non-rapid monomer-micelle exchange rate. This produces a concentration gradient along the droplet interface, leading to the action of opposing Marangoni forces on the internal flow. Also, the intrinsic surface rheology, which depends on both the chemical structure and the concentration of the surfactant, might be a contributing factor in the retardation. So, even at very high bulk concentration of Tween 20, the internal flow is not completely remobilized.

6.4.4 Effect of SDS on internal flow in a disk-shaped droplet in the squeezing regime (Ca = 0.001)

The effect of droplet shape on the internal flow is also investigated in this study. For this part, droplet shape is changed from slug like to disk shaped droplet. This droplet has a complete circular cross section at the depth wise middle plane of the droplet. This results in nearly negligible surface contact between the channel walls and the disk-shaped droplet. Consequently, the intensity of the two vortices due to liquid-wall friction induced inside the slug droplet at the middle plane is reduced significantly. This can be observed in Figure 6.5.

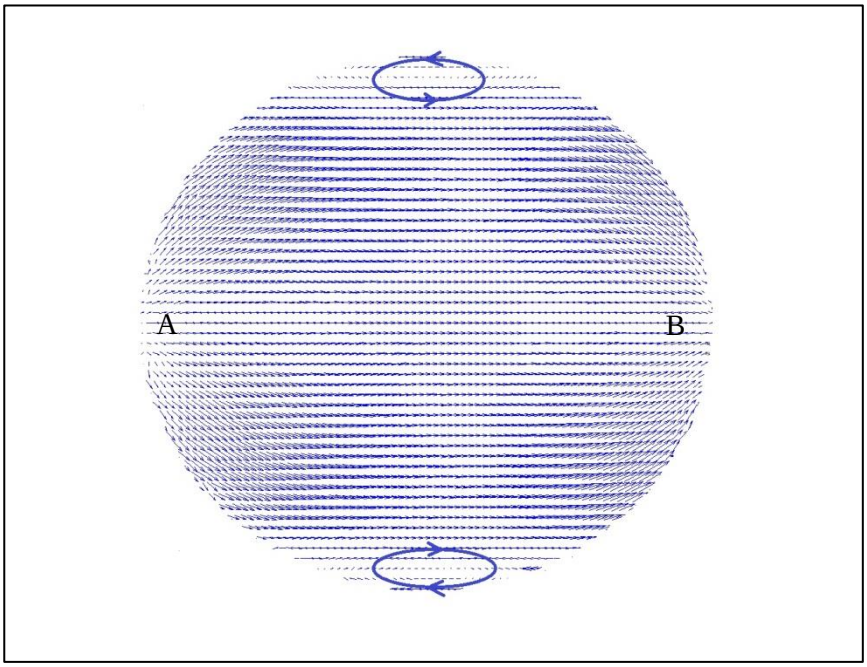

Figure 6.5: Internal flow fields inside the disk shaped droplet

It should be mentioned that this flow profile is at the depth wise middle plane. But, for the complete droplet, three-dimensional flow occurs inside the droplet. Flow enters the middle plane at region ‘A’ and leaves at region ‘B’, resulting in a 3-D flow.

The results for the vorticity inside the disk shaped droplet with increasing concentration of SDS at the squeezing regime are shown in Figure 6.6.

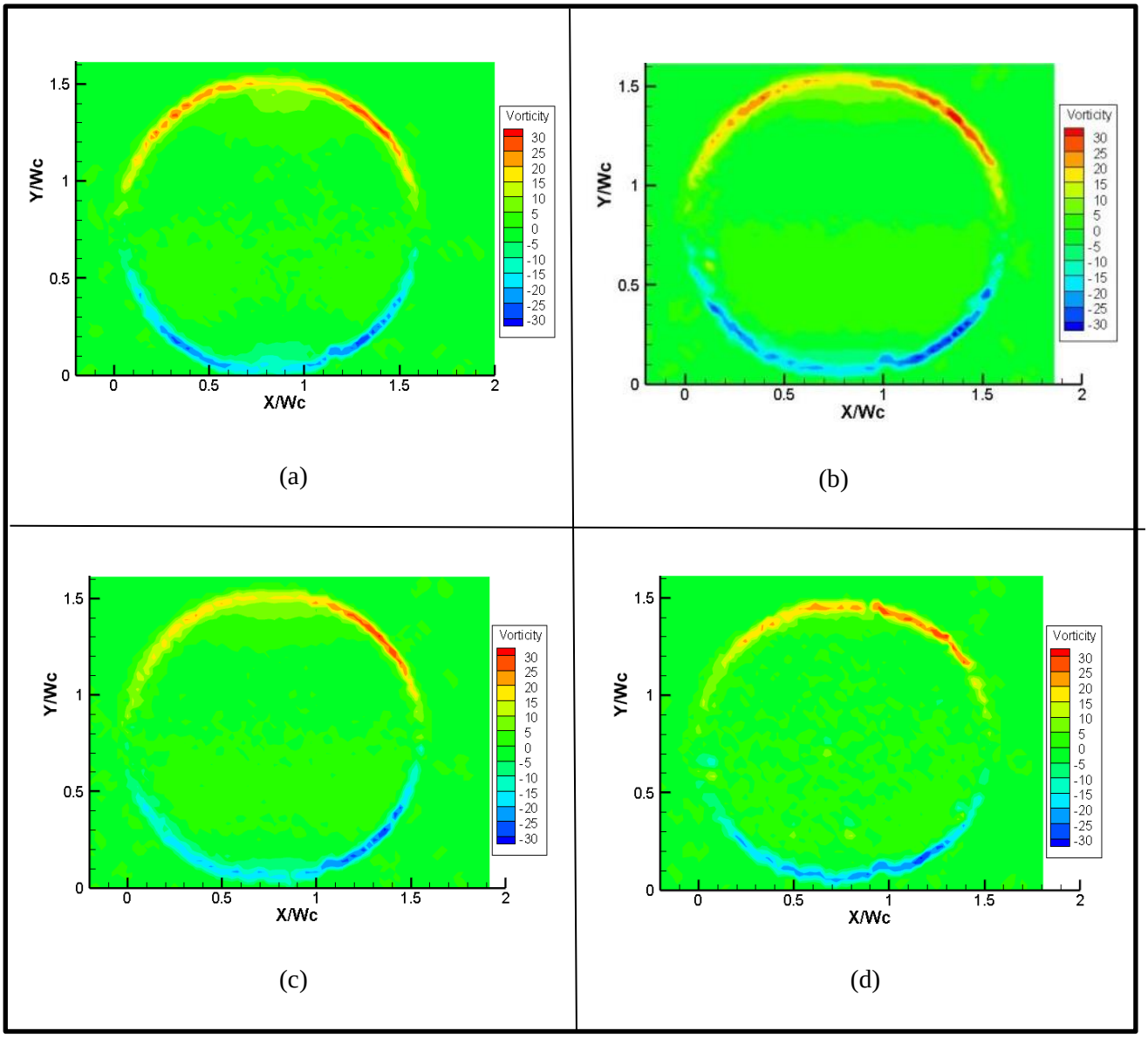

Figure 6.6: Vorticity map inside disk shaped droplet with increasing SDS concentration at squeezing regime (a) No SDS (b) below CMC (c) 2X CMC (d) 10X CMC

As can be observed in Figure 6.5, two small vortices are observed at the depth wise middle plane of the droplet. This is analogous to the two main vortices observed inside the slug droplet, with the difference being the size of the vortices. In the slug case, the vortices are induced due to the liquid-wall friction and are present along the length of the slug which is in contact with the channel walls. But in the case of disk-shaped droplets, the contact area between the droplet and the channel wall is negligible, which results in appearance of small vortices inside the droplet. In the condition where no surfactant is added, dimensionless vorticity in the range of 15-20 is present in the region of these vortices. Vortices of high intensity are present at the leading and trailing edge due to liquid-liquid interaction. Addition of SDS at concentration below CMC does not retard the internal flow significantly inside the droplet. This is in contrast to what is observed in the previous cases for the slug droplet. This can be attributed to the size of the vortices inside the droplet. In the slug case, the vortices are expanded along the slug length. This means that the monomers tend to deplete from the leading edge and accumulate at the trailing edge of the slug, if the retarding conditions are present inside the droplet. This results in action of opposing Marangoni stresses on the droplet which retard the internal flow. However, the retardation observed in the disk-shaped droplets on addition of SDS is very less as compared to the slug case. This can be attributed to the small size of vortices at the depth wise middle plane of the droplet. There might be some retardation present along these vortices, but is very less as compared to the slug case. Similar trend is observed at higher concentration (2-10X CMC) of SDS as well.

6.5 Conclusion

A µPIV system was used to examine the effect of surfactant concentration and size at two different droplet regimes, squeezing and transition. A T-junction generator was used to generate the droplets. Silicone oil was used as the continuous phase and water-glycerol solution was used as the dispersed phase. Two surfactants, SDS and Tween 20 were used at concentrations both below and above CMC value. In the later part of the study, the shape of the droplet was changed from slug to disk-shaped droplet and the effect of SDS concentration on this droplet shape was studied.

The experimental results indicate that the internal flow gets completely remobilized for higher concentration of SDS in slug droplet in the squeezing regime, but not in the transition regime. Higher concentration of Tween 20 is also not able to completely remobilize internal flow in the squeezing regime in slug droplets. The addition of surfactant has a negligible effect on the disk-shaped droplets as very less retardation is observed as compared to slug droplet.

Chapter 7: Conclusion and Future Work

7.1 Conclusion

The study of the effect of surfactant concentration on the internal flow fields inside a moving droplet is performed. µPIV technique is employed as it is a great tool to characterize internal flow due to its high spatial resolution. A rectangular PDMS micro-channel is fabricated using soft lithography technique. Silicone oil is used as the continuous phase and water-glycerol solution is used as the dispersed phase. Fluorescent particles of diameter = 1µm are added to the dispersed phase to observe the internal flow inside the moving droplet. Two different surfactants, SDS and Tween 20 are chosen as they allow a wide timescale of adsorption to be studied due to the relative difference in their size. The experimental system comprises of two sub-systems; droplet detection and triggering sub-system, and the µPIV sub-system. The experimental system is connected in such a manner that the droplet detection and triggering sub-system acts as an external actuator for the µPIV sub-system.

The study with SDS has been performed at two different droplet regimes, squeezing and transition. Also, the effect of surfactant concentration on droplet shape has been studied by comparing the results between the slug droplet and the disk-shaped droplet. It is observed that addition of SDS to slug droplet at the squeezing regime below CMC condition causes retardation

in the internal flow, which is primarily attributed to the action of opposing Marangoni forces. Increasing the SDS concentration to 2X CMC causes partial remobilization of the internal flow, and eventually at higher concentration (5X and 10X CMC), the internal flow gets completely remobilized. However, addition of SDS at higher concentration (5X and 10X CMC) to slug droplet at the transition regime does not attains complete remobilization. This can be attributed to the slow micellar break up kinetics of SDS as compared to the fast convective rate present inside the droplet at this regime. The addition of Tween 20 to the slug droplet at below CMC condition at the squeezing regime also causes retardation of the internal flow. But unlike SDS, complete remobilization is not observed at higher concentration (10X CMC) of Tween 20. This can be attributed to the slow desorption rate of Tween 20 due to its bigger size as compared to SDS. Finally, the effect of SDS in disk-shaped droplet is observed at the squeezing regime. It is observed that very less retardation is present in the internal flow inside the droplet as compared to the slug droplet. This can be attributed to the small size of the two main vortices inside the disk shaped droplet.

7.2 Outlook for future work

Every research work has its boundaries. Similarly, the work presented in this thesis also has a defined scope. This study attempted to observe the effect of surfactant concentration and size on different droplet shapes and at different droplet regimes. The current work showed some insights into this area and showed the potential of future work in this area. An attempt to list some potential work for the future is discussed briefly.

Mathematical modelling for the surfactant effect: It would be an interesting work to develop a mathematical model for surfactant effect on internal flow inside a moving droplet for the discussed experimental study. The model would relate the internal circulation velocity with the flow parameters (convection rate, liquid/wall drag etc.) and the surfactant parameters (concentration, size, exchange kinetics etc.)

Observation of the continuous phase: The work in this study is limited to the flow visualization of the dispersed phase only. An extension to this can be internal flow visualization in the continuous phase, while the surfactant is added to the dispersed phase. However, a challenge associated with this approach is that fluorescent particles which can be added to silicone oil are not commercially available.

Appendix A: Uncertainty Analysis

A.1 Introduction

Error is a property of the measurement, while uncertainty is a property of the result. Uncertainty is a prediction whereas statistics is applied to the data which exists. Uncertainty can be determined, depending on how accurately is the test knowledge, equipment expertise, measured variables and procedures known.

Absolute uncertainty is given as:

$$x_i = X_i \pm \Delta U_x \qquad \text{(P\%)} \tag{A.1}$$

where x_i is the input data, X_i is the sample mean and ΔU_x is the uncertainty in the sample mean with P% probability. Uncertainty analysis is a method used to quantify ΔU_x [73].

Uncertainty analysis can be performed at three stages of an experiment:

A1.1 Design stage uncertainty (zero order uncertainty)

This comprises of the initial analysis performed prior to the experiment. It is useful for selecting instruments, measurement technique and obtaining approximate uncertainty likely in measured data. It assumes that the uncertainty is entirely due to the instrument resolution. Uncertainty in a measurement is due to:

1. Instrument accuracy (U_c)

2. Random error from reading instrument (U_o).

As a rule of thumb, $U_o = \pm 0.5$*resolution (95% confidence) [73].

Design stage uncertainty, $U_d = \pm\sqrt{U_o^2 + U_c^2}$. This is also considered as bias uncertainty.

A1.2 Shake down testing (first-order uncertainty)

In first order uncertainty, the temporal variations are also included. The display for each instrument is assumed to vary stochastically about the stationary mean. First order uncertainty will include time variation in the display along with the instrument reading uncertainty. Design stage uncertainty was a pre-experiment estimate of first order uncertainty.

$$U_1 = \pm t.S_X \tag{A.2}$$

where U_1 is the first order uncertainty, t is value from student`s t-distribution and $S_X$ is the sample standard deviation of the mean. Student`s t is a correction for finite value statistics accounting for small sample sizes. Any higher order uncertainty incorporates the randomness from the various sources and is also considered as random uncertainty [73].

A1.3 Presented results (N^{th} order uncertainty)

N^{th} order uncertainty includes all sources of error. This allows direct analogy among results of identical tests using different set of equipment at different testing sites.

$$U_N = \pm\left[U_C^2 + \left(\sum_{i=1}^{N-1} U_i^2\right)\right]^{1/2} \tag{A.3}$$

A.2 µPIV uncertainty

A2.1 Design stage uncertainty

There are two components of design stage uncertainty: instrument uncertainty (U_c) and reading error (U_o)

By rule of thumb, $U_o = \pm 0.5$*resolution (95% confidence)

1. **Syringe Pump**: Pump 33 Harvard Apparatus

   Resolution= 0.0004 µl/hr

   $U_o = \pm 0.0002$ µl/hr = 0.0000033 µl/min

   Accuracy = ± 0.35 %

   For flow rate of 35 µl/min

   $U_c = \pm 0.0035*35 = \pm 0.1225$ µl/min

   $U_d = \pm (U_o^2 + U_c^2)^{1/2}$

   $= \pm 0.1225$ µl/min (95% confidence)

2. **Micro Channel**:

   Resolution= 2 µm

   $U_o = \pm 1$ µm

   Accuracy = ± 5 %

   For width of 200 µm

   $U_c = \pm 0.05*200 = \pm 10$ µm

   $U_d = \pm (U_o^2 + U_c^2)^{1/2}$

   $= \pm 10.05$ µm (95% confidence)

3. **Nd-Yag Laser**: New Wave research (15 mJ)

   Resolution= 5 ps

   $U_o = \pm 0.5*5$ ps = ± 2.5 ps

Accuracy = ± 1 ns = U_c

$U_d = \pm (U_o^2 + U_c^2)^{1/2}$ = ± 1000 ps (95% confidence)

4. **Synchroniser**: IDT vision Timing hub
   U_o = ± 0.5 * Resolution
   = ± 0.5*20 ns = ± 10 ns

   Accuracy = ± 20 ns = U_c

   $U_d = \pm (U_o^2 + U_c^2)^{1/2}$
   $= \pm (400+100)^{1/2}$
   = ± 22.36 ns (95% confidence)

A2.2 Higher order uncertainty

There are several uncertainties associated with the µPIV technique. The main sources of uncertainties are:

1. Fluorescent particle sources
2. Optical sources
3. Image recording and sensor sources [24]

The Reynolds number for the flow is calculated as

$$Re = \frac{\rho \times w \times U}{\mu} \tag{A.4}$$

where, ρ= density of the continuous phase (Si oil) = 930 kg/m^3

w= width of the channel (200 µm)

U= mean velocity of the flow = 0.0032 m/s

µ= viscosity of the continuous phase = 10 mPas

The value of Reynolds number turns out to be 0.06. Since this is much less than 1, the drag force (F_D) on the particles is considered only due to Stokes drag.

$$F_D = 3 \times \pi \times \mu_f \times \left(V_f - V_p\right) \times d_p \tag{A.5}$$

where, V_f = velocity of the dispersed phase

μ_f = viscosity of the continuous phase

V_p = velocity of the seeding particles

d_p = diameter of the seeding particles

A time constant factor for the tracer particles is given as

$$\tau = \frac{\rho_f \times d_p^2}{18 \times \mu_f} \tag{A.6}$$

which turns out be in the order of nanoseconds. This means that the tracer particles take very less time to acquire the velocity of the droplets and there is no uncertainty related to the tracer particles following the flow inside the droplet. This is because it takes about half an hour to stabilize the droplets in the micro channel and the flow is quite steady.

Another uncertainty associated with the motion of the particles is caused due to Brownian motion. This is associated with the random diffusive motion of the tracer particles. Einstein equation [1] is used to estimate the Brownian motion for particles:

$$D_b = \frac{K \times T_a}{3 \times \pi \times \mu_f \times d_p} \tag{A.7}$$

where D_b is the particles diffusivity due to the Brownian motion , K is the Boltzmann constant, T_a is the absolute temperature (K) of the fluid, μ_f is the fluid viscosity and d_p is the particle

diameter. The uncertainty in the result due to the Brownian motion is reduced by taking the particle displacement to be very small between two image pairs and averaging the results.

Table A-1provides the different types of uncertainties associated with the µPIV studies [24].

Table A-1: Different types of uncertainties associated with the µPIV studies

Uncertainty Association	Uncertainty estimate	Type
Particle flow	$\tau = \frac{\rho_f \times d_p^2}{18 \times \mu_f}$	Bias
Brownian motion	$D_b = \frac{K \times T_a}{3 \times \pi \times \mu_f \times d_p}$	Random
Accuracy	$\delta_d = \frac{d_e}{M}\frac{1}{10}$	Bias
Background noise	-	Random
Refractive index mismatch	-	Bias
Statistical cross correlation	-	Random
Optical distortions	-	Bias

There is also variation in the width ‘w’ of the microchannel. This is due to the fact that PDMS swells when it comes in contact with silicone oil. For initial width of 200 µm, the maximum variation in the width of the channel has been measured as approximately 12 µm [24].

The most significant contributor of uncertainty in the velocity measurements is the spatial location of the particles. For the current study, this uncertainty variation is estimated to be between 4% to 8% for the µ-PIV experiments. [24]

References

1 Nguyen, Nam-Trung, and Steven T. Wereley. *Fundamentals and applications of microfluidics*. Artech House, 2002.

2 Whitesides, George M. "The origins and the future of microfluidics." *Nature*442.7101 (2006): 368-373.

3 Bruus, Henrik. *Theoretical Microfluidics*. New York: OUP Oxford, 2008.

4 Beebe, David J., Glennys A. Mensing, and Glenn M. Walker. "Physics and applications of microfluidics in biology." *Annual review of biomedical engineering* 4.1 (2002): 261-286.

5 Demello, Andrew J. "Control and detection of chemical reactions in microfluidic systems." *Nature* 442.7101 (2006): 394-402.

6 Dittrich, Petra S., Kaoru Tachikawa, and Andreas Manz. "Micro total analysis systems. Latest advancements and trends." *Analytical chemistry* 78.12 (2006): 3887-3908.

7 Chin, Curtis D., Vincent Linder, and Samuel K. Sia. "Lab-on-a-chip devices for global health: Past studies and future opportunities." *Lab on a Chip* 7.1 (2007): 41-57.

8 Yi, Changqing, et al. "Microfluidics technology for manipulation and analysis of biological cells." *Analytica Chimica Acta* 560.1 (2006): 1-23.

9 Stroock, Abraham D., and George M. Whitesides. "Components for integrated poly (dimethylsiloxane) microfluidic systems." *Electrophoresis* 23.20 (2002): 3461-3473.

10 Duffy, David C., et al. "Rapid prototyping of microfluidic systems in poly (dimethylsiloxane)." *Analytical chemistry* 70.23 (1998): 4974-4984.

11 Zhou, Jinwen, et al. "Surface modification for PDMS-based microfluidic devices." *Electrophoresis* 33.1 (2012): 89-104.

12 Lee, Jessamine Ng, Cheolmin Park, and George M. Whitesides. "Solvent compatibility of poly (dimethylsiloxane)-based microfluidic devices." *Analytical chemistry* 75.23 (2003): 6544-6554.

13 Cheung, Perry, Kazumi Toda-Peters, and Amy Q. Shen. "In situ pressure measurement within deformable rectangular polydimethylsiloxane microfluidic devices." *Biomicrofluidics* 6.2 (2012): 026501.

14 Almutairi, Zeyad, Carolyn L. Ren, and Leonardo Simon. "Evaluation of polydimethylsiloxane (PDMS) surface modification approaches for microfluidic applications." *Colloids and Surfaces A: Physicochemical and Engineering Aspects* 415 (2012): 406-412.

15 Pittman, Jason L., Charles S. Henry, and S. Douglass Gilman. "Experimental studies of electroosmotic flow dynamics in microfabricated devices during current monitoring experiments." *Analytical chemistry* 75.3 (2003): 361-370.

16 Glawdel, Tomasz, Caglar Elbuken, and Carolyn L. Ren. "Droplet formation in microfluidic T-junction generators operating in the transitional regime. II. Modeling." *Physical Review E* 85.1 (2012): 016323.

17 Teh, Shia-Yen, et al. "Droplet microfluidics." *Lab on a Chip* 8.2 (2008): 198-220.

18 Shui, Lingling, Jan CT Eijkel, and Albert van den Berg. "Multiphase flow in microfluidic systems–Control and applications of droplets and interfaces."*Advances in Colloid and Interface Science* 133.1 (2007): 35-49.

19 Günther, Axel, et al. "Micromixing of miscible liquids in segmented gas-liquid flow." *Langmuir* 21.4 (2005): 1547-1555.

20 Song, Helen, et al. "Experimental test of scaling of mixing by chaotic advection in droplets moving through microfluidic channels." *Applied Physics Letters*83.22 (2003): 4664-4666.

21 Geng, Tao, Richard Novak, and Richard A. Mathies. "Single-cell forensic short tandem repeat typing within microfluidic droplets." *Analytical chemistry* 86.1 (2013): 703-712.

22 Kinoshita, Haruyuki, et al. "Three-dimensional measurement and visualization of internal flow of a moving droplet using confocal micro-PIV." *Lab on a Chip*7.3 (2007): 338-346.

23 Glawdel, Tomasz. *Droplet Production and Transport in Microfluidic Networks with Pressure Driven Flow Control*. Ph.D thesis. University of Waterloo, 2012.

24 Almutairi, Zeyad. *Experimental Studies of the Hydrodynamics of Liquid Droplet Generation and Transport in Microchannels*. Ph.D thesis. University of Waterloo, 2014.

25 Baroud, Charles N., Francois Gallaire, and Rémi Dangla. "Dynamics of microfluidic droplets." *Lab on a Chip* 10.16 (2010): 2032-2045.

26 Oh, Seong-Geun, Scott Paul Klein, and D. O. Shah. "Effect of micellar life-time on the bubble dynamics in sodium dodecyl sulfate solutions." *AIChE journal*38.1 (1992): 149-152.

27 Hudson, Steven D., et al. "Microfluidic interfacial tensiometry." *Applied Physics Letters* 87.8 (2005): 81905-81905.

28 Pipe, Christopher J., and Gareth H. McKinley. "Microfluidic rheometry."*Mechanics Research Communications* 36.1 (2009): 110-120.

29 Funfak, Anette, et al. "Monitoring cell cultivation in microfluidic segments by optical pH sensing with a micro flow-through fluorometer using dye-doped polymer particles." *Microchimica Acta* 164.3-4 (2009): 279-286.

30 Clausell-Tormos, Jenifer, et al. "Droplet-based microfluidic platforms for the encapsulation and screening of mammalian cells and multicellular organisms." *Chemistry & biology* 15.5 (2008): 427-437.

31 Liau, Albert, et al. "Mixing crowded biological solutions in milliseconds." *Analytical chemistry* 77.23 (2005): 7618-7625.

32 Sackmann, Eric K., Anna L. Fulton, and David J. Beebe. "The present and future role of microfluidics in biomedical research." *Nature* 507.7491 (2014): 181-189.

33 Christopher, G. F., and S. L. Anna. "Microfluidic methods for generating continuous droplet streams." *Journal of Physics D: Applied Physics* 40.19 (2007): R319.

34 Glawdel, Tomasz, and Carolyn L. Ren. "Global network design for robust operation of microfluidic droplet generators with pressure-driven flow." *Microfluidics and nanofluidics* 13.3 (2012): 469-480.

35 Van Steijn, V., M. T. Kreutzer, and C. R. Kleijn. "Velocity fluctuations of segmented flow in microchannels." *Chemical Engineering Journal* 135 (2008): S159-S165.

36 Christopher, Gordon F., et al. "Experimental observations of the squeezing-to-dripping transition in T-shaped microfluidic junctions." *Physical Review E* 78.3 (2008): 036317.

37 Garstecki, Piotr, et al. "Formation of droplets and bubbles in a microfluidic T-junction—scaling and mechanism of break-up." *Lab on a Chip* 6.3 (2006): 437-446.

38 Xu, J. H., et al. "Correlations of droplet formation in T-junction microfluidic devices: from squeezing to dripping." *Microfluidics and Nanofluidics* 5.6 (2008): 711-717.

39 Fu, Taotao, et al. "Squeezing-to-dripping transition for bubble formation in a microfluidic T-junction." *Chemical engineering science* 65.12 (2010): 3739-3748.

40 Korczyk, Piotr M., et al. "Effects of unsteadiness of the rates of flow on the dynamics of formation of droplets in microfluidic systems." *Lab on a Chip* 11.1 (2011): 173-175.

41 Rosen, Milton J. and Joy T. Kunjappu. *Surfactants and Interfacial Phenomena.* New Jersey: John Wiley & Sons, 2012.

42 De Gennes, Pierre-Gilles. "Wetting: statics and dynamics." *Reviews of modern physics* 57.3 (1985): 827.

43 Sharma, Sanjiv, et al. "Droplet-based microfluidics." *Microfluidic Diagnostics*. Humana Press, 2013. 207-230.

44 Chen, I-Jane, and Ernö Lindner. "The stability of radio-frequency plasma-treated polydimethylsiloxane surfaces." *Langmuir* 23.6 (2007): 3118-3122.

45 Raffel, Markus, Christian E. Willert, and Jürgen Kompenhans. *Particle image velocimetry: a practical guide*. Springer, 2013.

46 Adrian, Ronald J. "Twenty years of particle image velocimetry." *Experiments in fluids* 39.2 (2005): 159-169.

47 Westerweel, J. "Fundamentals of digital particle image velocimetry."*Measurement science and technology* 8.12 (1997): 1379.

48 Lindken, Ralph, et al. "Micro-particle image velocimetry (μPIV): recent developments, applications, and guidelines." *Lab on a Chip* 9.17 (2009): 2551-2567.

49 Wereley, Steven T., and Carl D. Meinhart. "Recent advances in micro-particle image velocimetry." *Annual Review of Fluid Mechanics* 42 (2010): 557-576.

50 Yamaguchi, Eiichiro, Bradford J. Smith, and Donald P. Gaver III. "μ-PIV measurements of the ensemble flow fields surrounding a migrating semi-infinite bubble." *Experiments in fluids* 47.2 (2009): 309-320.

51 Kim, B. J., Y. Z. Liu, and H. J. Sung. "Micro PIV measurement of two-fluid flow with different refractive indices." *Measurement science and technology* 15.6 (2004): 1097.

52 Budwig, R. "Refractive index matching methods for liquid flow investigations." *Experiments in fluids* 17.5 (1994): 350-355.

53 van Steijn, Volkert, Michiel T. Kreutzer, and Chris R. Kleijn. "μ-PIV study of the formation of segmented flow in microfluidic T-junctions." *Chemical Engineering Science* 62.24 (2007): 7505-7514.

54 Günther, Axel, and Klavs F. Jensen. "Multiphase microfluidics: from flow characteristics to chemical and materials synthesis." *Lab on a Chip* 6.12 (2006): 1487-1503.

55 Bourdon, Christopher J., Michael G. Olsen, and Allen D. Gorby. "The depth of correlation in micro-PIV for high numerical aperture and immersion objectives."*Journal of fluids engineering* 128.4 (2006): 883-886.

56 Shinohara, Kyosuke, et al. "High-speed micro-PIV measurements of transient flow in microfluidic devices." *Measurement science and Technology* 15.10 (2004): 1965.

57 Wang, Cheng, Nam-Trung Nguyen, and Teck Neng Wong. "Optical measurement of flow field and concentration field inside a moving nanoliter droplet." *Sensors and Actuators A: Physical* 133.2 (2007): 317-322.

58 Malsch, D., et al. "μPIV-analysis of Taylor flow in micro channels." *Chemical Engineering Journal* 135 (2008): S166-S172.

59 Baret, Jean-Christophe. "Surfactants in droplet-based microfluidics." *Lab on a Chip* 12.3 (2012): 422-433.

60 Dominguez, Ana, et al. "Determination of critical micelle concentration of some surfactants by three techniques." *Journal of Chemical Education* 74.10 (1997): 1227.

61 “Critical Micelle Concentration” *Kruss*. KRUSS GmbH, n.d. Web. 20 April 2015. <http://www.kruss.de/services/education-theory/glossary/cmc/>

62 Rosen, Milton J., and Joy T. Kunjappu. *Surfactants and interfacial phenomena*. John Wiley & Sons, 2004.

63 Seemann, Ralf, et al. "Droplet based microfluidics." *Reports on progress in physics* 75.1 (2012): 016601.

64 Stebe, Kathleen J., Shi-Yow Lin, and Charles Maldarelli. "Remobilizing surfactant retarded fluid particle interfaces. I. Stress-free conditions at the interfaces of micellar solutions of surfactants with fast sorption kinetics."*Physics of Fluids A: Fluid Dynamics (1989-1993)* 3.1 (1991): 3-20.

65 Stebe, Kathleen J., and Charles Maldarelli. "Remobilizing surfactant retarded fluid particle interfaces: ii. controlling the surface mobility at interfaces of solutions containing surface active components." *Journal of colloid and interface science* 163.1 (1994): 177-189.

66 Martin, Jeffrey D., and Steven D. Hudson. "Mass transfer and interfacial properties in two-phase microchannel flows." *New Journal of Physics* 11.11 (2009): 115005.

67 Wang, K., et al. "Determination of dynamic interfacial tension and its effect on droplet formation in the T-shaped microdispersion process." *Langmuir* 25.4 (2009): 2153-2158.

68 Ruiz, C. Carnero, L. Díaz-López, and J. Aguiar. "Micellization of sodium dodecyl sulfate in glycerol aqueous mixtures." *Journal of Dispersion Science and Technology* 29.2 (2008): 266-273.

69 Molecular Probes, Inc. *Working with FluoSpheres Fluorescent Microspheres*, n.d. Web. 10 November 2014.

70 “Plasma Cleaner”, *Harrick Plasma*. Harrick Plasma Company, n.d. Web. 15 March 2014 <https://camtools.cam.ac.uk/access/content/group/d4fe6800-4ce2-4bad-8041-957510e5aaed/Public/3YP-µfluidics/Manuals/PlasmaCleaner.pdf>

71 Jakiela, Slawomir, et al. "Discontinuous transition in a laminar fluid flow: a change of flow topology inside a droplet moving in a micron-size channel."*Physical review letters* 108.13 (2012): 134501.

72 Ma, Shaohua, et al. "On the flow topology inside droplets moving in rectangular microchannels." *Lab on a Chip* 14.18 (2014): 3611-3620.

73 Moffat, R. J. "Contributions to the theory of single-sample uncertainty analysis." *ASME, Transactions, Journal of Fluids Engineering* 104.2 (1982): 250-58.